ASSESSMENT OF RADIATION DOSE TO PATIENTS DURING SINGLE PHOTON EMISSION COMPUTED TOMOGRAPHY (SPECT) ^{99m}Tc-SESTAMIBI MYOCARDIAL PERFUSION IMAGING (MPI) IN NIAMEY- NIGER.

This thesis is presented to the

DEPARTMENT OF MEDICAL PHYSICS
SCHOOL OF NUCLEAR AND ALLIED SCIENCES
UNIVERSITY OF GHANA

BY

ADAMOU SOLI IDRISSA
(10509438)
B.Sc. (University of Niamey, 2009)

IN PARTIAL FULFILLMENT OF THE REQUIREMENTS FOR THE AWARD OF A

MASTER OF PHILOSOPHY

IN

MEDICAL PHYSICS

JULY, 2016

DECLARATION

This thesis is the result of research work undertaken by ADAMOU SOLI IDRISSA in the Department of Medical Physics, School of Nuclear and Allied Sciences, University of Ghana, under the supervision of Prof. A. W. K. Kyere, Dr. I. K. Wilson and Dr. F. Hasford

Sign…… Date……

Idrissa ADAMOU SOLI

(Student)

Supervisor's Declaration

We hereby declare that the preparation and presentation of this thesis were supervised in accordance with guidelines on supervision of thesis laid down by the University of Ghana

Sign…… Date……

Prof. A. W. K. Kyere

(Principal supervisor)

Sign…… Date……

Dr. I. K. Wilson

(Co-Supervisor)

Sign…… Date……

Dr. F. Hasford

(Co-Supervisor)

ABSTRACT

Radiation absorbed dose for patients undergoing myocardial perfusion has been calculated for technetium-99m Hexakis-2-methoxy-2-methylpropyl-isonitrile (^{99m}Tc-Sestamibi) at the Nuclear Medicine Department of Abdou Moumouni University.

Thirty patients were scanned and image quantification was achieved using MedisoInterViewXP® software. An activity of370 MBq (10 mCi) of ^{99m}Tc-Sestamibi was administered for stress and 1110 MBq (30 mCi) for rest. A 256 x 1024 matrix size and a speed of 250 mm per minute were used to acquire the whole body image at 10 minutes, 2 hours and 4 hours after injection of ^{99m}Tc-Sestamibi for heart, liver and kidneys quantifications and 10 minutes, 20 minutes and 2 hours for urinary bladder quantification. The activities of the heart, liver, kidneys and urinary bladder were determined using the conjugate view method. The uptake of ^{99m}Tc-Sestamibi in the heart, liver and kidneys were respectively 2.17%, 6.53% and 5%, 10 minutes after injection and were in good agreement with the work of Wacker's et al of respectively 1.5±0.4%, 5.9±2.9% and 10.6±2.2% 5 minutes after injection.

The cumulative activities for the heart, liver, kidneys and urinary bladder were respectively30.81MBq/h, 74.98MBq/h, 39.09MBq/h, 136.25MBq/h for the stress and 86.78MBq/h, 244.77MBq/h, 108.76MBq/h and 338.80MBq/h for the rest.

The difference in the absorbed dose values obtained was less than 10% except for kidneys which was about 15% for both female and male patients. Both methods found a relatively high absorbed dose per unit of injected activity (mGy/MBq) for urinary bladder and ovaries as target-organs for female patients.

Also the uncertainties were in the good agreement according to Stabin.

DEDICATION

To the Almighty God,

Who has brought this research work to a successful end.

To my parents ADAMOU SOLI and SAHIYAMAIGARI for giving birth to me and supporting me throughout their life, rest in peace

This research work is dedicated

To my mother SAHIYA MAIGARI

To my father ADAMOU SOLI

To my wife Hadizatou AMADOU ALZOUMA

To the Director of Radioisotopes Institute, Dr ALI ADA

To the Chief of Nuclear Medicine Department, Dr Iliassou TAHIROU

To Prof. Ben Mohamed Abdelkrim, Radioisotopes Institute

To the Chief of Nuclear Physics, Dr SOUMANA Salifou, Radioisotopes Institute

To Dr ILLA SALIFOU Illa, Radioisotopes Institute

To all my class mate

ACKNOWLEDGEMENTS

First and foremost, I will give thanks to Abdou Moumouni University, the Radioisotopes Institute and Belgium technical cooperation for sponsoring my two years education. Special thanks go to the Director of the Radioisotopes Institute, Dr ALI ADA and the Chief of Nuclear Medicine Department, Dr Iliassou TAHIROU for their encouragement.

I extend my utmost gratitude to Prof A. W. K. Kyere and Dr. I. K. Wilson, for their understanding, encouragement and personal guidance that have provided a good basis for this thesis.

Thanks to Prof, J. H. AMUASI, Prof C. SCHANDORF and Prof J. J. FLETCHER, for their precious lectures and advice.

My special thanks to Dr F. Hasford for his support and contribution for the success of this work.

Thanks to the personal of Radioisotopes Institute, friends, colleagues and lecturers of School of Nuclear and Allied Sciences, for their priceless support and encouragement.

Last but not the least, to those who indirectly contributed in this research, your kindness means a lot to me. Thank you very much.

TABLE OF CONTENTS

DECLARATION I

ABSTRACT II

DEDICATION III

ACKNOWLEDGEMENTS IV

TABLE OF CONTENTS V

LIST OF FIGURES VIII

LIST OF TABLES X

LIST OF ABBREVIATIONS AND SYMBOLS XI

CHAPTER ONE: INTRODUCTION 1

1.1 BACKGROUND 1

1.2 STATEMENT OF THE PROBLEM 3

1.3 OBJECTIVES 5

1.4 RELEVANCE AND JUSTIFICATION 6

1.5 SCOPE AND LIMITATION 6

1.6 ORGANISATION OF THESIS 7

CHAPTER TWO: LITERATURE REVIEW 8

2.1 THE BASICS OF INTERNAL DOSIMETRY 9

2.1.1 Radiation dose assessment 12

2.1.2 Evolution of Dosimetric Formalisms 17

2.1.3 Planar methods for quantification 19

2.1.4 Quantification of tomographic data 26

2.2 RADIOPHARMACEUTICALS 27

2.2.1 Uncertainty of Biokinetic Model of Radiopharmaceuticals 27

2.2.2 Radiopharmaceuticals used in diagnostic imaging procedures 28

Table 2.1 Standard Myocardial perfusion SPECT patient radiation doses: ..32

2.3. INDICATIONS FOR MYOCARDIAL PERFUSION IMAGING (MPI) 32

2.4 IMAGE ACQUISITION 33

Instrumentation 33

2.4.3 SPECT Imaging 33

Basic principle 34

CHAPTER THREE: MATERIALS AND METHOD.....37

3.1 EQUIPMENT AND SOFTWARE.....37

3.1.1 The Mediso gamma camera system.....37

3.1.2 The InterViewXP®software.....38

3.1.3 OLINDA software 40

3.2 METHODOLOGY 42

3.2.1 Wholebody scan 42

3.2.2 Data collection.....43

Table 3.1: Biodata and injected activity of 30 patients 44

3.2.3 Quantitative assessment.....46

3.2.4 Conversion of counts into activity.....46

3.2.5 Biokinetic model.....49

3.2.6 Determination of the residence time.....51

3.2.7 Dose calculation 53

Table 3.2: Estimated radiation dose to certain organs according to Mirdose3 using ^{99m}Tc-Sestamibi 53

3.2.8 Determination of the Uncertainty of Biokinetic models for ^{99m}Tc-Sestamibi 54

CHAPTER FOUR: RESULTS AND DISCUSSION.....55

4.1 INTRODUCTION.....55

4.2 RESULTS.....55

4.2.1 Body and organs thickness 55

Table 4.1: Average thickness for the body and organs thickness for 10 sized patient CT scan.....56

4.2.2 Activity of the source- organs 56

Table 4.2: Estimated radionuclide activities in organs for patients, ten minutes post-injection of 10 mCi Tc-99m Sestamibi 58

Table 4.3: Estimated bladder activity after injection of 10 mCi Tc-99m Sestamibi 59

Table 4.4: Estimated organs activities for patients, 120 minutes post injection of 10 mCi Tc-99m Sestamibi 60

Table 4.5: Estimated organs activities for the patients 240 minutes 61
post-injection of 10 mCi Tc-99m Sestamibi 61
Table 4.6: Estimated organs activities for the patients 10 minutes post injection of 30 mCi Tc-99m Sestamibi 63
Table 4.7: Estimated bladder activity after injection of 30 mCi Tc-99m Sestamibi 64
Table 4.9: Estimated organs activities for the patients 240 minutes post-injection of 30 mCi Tc-99m Sestamibi 67
4.2.3 Cumulative activity estimation 69
4.2.4 Residence time of ^{99m}Tc-Sestamibi in the heart, liver, kidneys and bladder during myocardial perfusion imaging (MPI) 74
Table 4.10: Calculation of residence time of the heart, liver, kidneys and bladder 74
4.2.5 ^{99m}Tc-Sestamibi Biokinetic model 75
4.2.6 Absorbed dose in different organs 76
Table 4.11: Comparison of Absorbed dose per administered activity with OLINDA and MIRDOSE 3 76
4.2.7 Estimation of the uncertainties 78
5.1 CONCLUSION 81
5.2 RECOMMENDATIONS 83
REFERENCES 84

LIST OF FIGURES

Figure 2.1: Evolution of dosimetric formalism.....17

Figure 2.3: Energy spectrum for the 140 keV 99m-Tc.....23

Figure 2.4: Filtered back projection.....35

Figure 2.5: Attenuation correction.....36

Figure 3.1: Mediso gamma camera.....38

Figure 3.2: ROI selection.....39

Figure 3.3: Thickness measurement.....40

Figure 3.4: OLINDA input form.....41

Figure 3.5: Whole-body scan.....43

Figure 3.6: Determination of the system calibration factor.....48

Figure 3.7: Compartmental diagram.....49

Figure 3.8: protocol for estimating residence time.....52

Figure 4.1: Radionuclide activities in the heart, liver and kidneys.....68

Figure 4.2: Activity in the bladder.....69

Figure 4.3.Cumulative activity estimation in the heart after injection of 10 mCi of ^{99m}Tc-Sestamibi.....70

Figure 4.4. Heart cumulative activity estimation after injection of 30 mCi of ^{99m}Tc-Sestamibi.....70

Figure4.5 Liver cumulative activity estimation after injection for 10 mCi of ^{99m}Tc-Sestamibi.....71

Figure4.6 Liver cumulative activity estimation after injection of 30 mCi of ^{99m}Tc-Sestamibi.....71

Figure4.7 Kidneys cumulative activity estimation after injection of 10 mCi of ^{99m}Tc-Sestamibi.....72

Figure 4.8 Kidneys cumulative activity estimation after injection of 30 mCi of ^{99m}Tc-Sestamibi.....72

Figure 4.9 Bladder cumulative activity estimation after injection of 10 mCi of ^{99m}Tc-Sestamibi.....73

Figure 4.10 Bladder cumulative activity estimation after injection of 30 mCi of ^{99m}Tc-Sestamibi.....73

Figure 4.11: Time activity curve simulation for ^{99m}Tc-Sestamibi for blood, liver, kidney and bladder.....75

Urinary bladder absorbed dose per administered activity for females' patient is relatively high and consequently the absorbed dose to the ovaries is also high.....77

Figure 4.13: Absorbed dose per administered activity for male.....77

LIST OF TABLES

Table 2.1 Standard Myocardial perfusion SPECT patient radiation doses:.....32

Table 3.1: Biodata and injected activity of 30 patients.....44

Table 3.2: Estimated radiation dose to certain organs according to Mirdose3 using ^{99m}Tc-Sestamibi 53

Table 4.1: Average thickness for the body and organs thickness for 10 sized patient CT scan 56

Table 4.2: Heart, liver and kidneys activities 10 minutes post-injection of 10 mCi Tc-99m Sestamibi.....58

Table 4.3: bladder activity after injection of 10 mCi Tc-99m Sestamibi 59

Table 4.4: Heart, liver and kidneys activities for the patients 2 hours post-injection of 10 mCi Tc-99m Sestamibi 60

Table 4.5: Heart, liver and kidneys activities for the patients 4 hours post-injection of 10 mCi Tc-99m Sestamibi 61

Table 4.6: Heart, liver and kidneys activities for the patients 10 minutes post-injection of 30 mCi Tc-99m Sestamibi.....63

Table 4.7: Bladder activity after injection of 30 mCi Tc-99m Sestamibi.....64

Table 4.8: Heart, liver and kidneys activities for the patients 120 minutes post-injection of 30 mCi Tc-99m Sestamibi.....65

Table 4.9: Heart, liver and kidneys activities for the patients 240 minutes post-injection of 30 mCi Tc-99m Sestamibi.....67

Table 4.10: Calculation of residence time of the Heart, liver, kidneys and Bladder ...74

Table 4.11: Comparison of Absorbed dose per administered activity with OLINDA and MIRDOSE 3.....76

Table 4.12 Estimation of uncertainties of the Heart, liver, kidneys and Bladder 79

LIST OF ABBREVIATIONS AND SYMBOLS

3-D	Three-Dimensional
Ã	Cumulated activity
CLS	Counts within the Lower Scatter windows
Cpp	Count recorded within the Photopeak window
CT	Computed Tomography
Cts	Counts
CUS	Counts within the Upper Scatter windows
D	Mean absorbed dose,
DF	Dose Factor
DICOM	Digital Imaging and Communications in Medicine
EANM	European Association of Nuclear Medicine
f	fraction of administered activity
FOV	Field Of View
FS	Scaling Factor
Gy	Gray
H	Dose equivalent
IAEA	International Atomic Energy Agency
ICRP	International Commission on Radiological Protection

keV	Kilo electron-volt
LEHR	Low-Energy High Resolution
MBq	Mega Becquerel
mCi	Milli Curie
MIRD	Medical Internal Radiation Dose
Mo-99	Molybdenum-99
MPI	Myocardial Perfusion Imaging
NaI(Tl)	Sodium Iodine dope with Thallium
PET	Positron Emission Tomography
PMT	Photomultiplier tubes
Q	Quality factor
QA	Quality Assurance
ROI	Regions of Interest
S	Dose conversion factors
SEE	Specific Effective Energy
SPECT	Single Photon Emission Computed Tomography
SUVs	Standardized Uptake Values
Tb	Biological half-life,
Tc-99mSestamibi	Technetium-99m Hexakis-2-methoxy-2-methylpropyl-isonitrile

Te Effective half-life,

Tp, Physical half-life,

W_R Radiation weighting factor,

CHAPTER ONE: INTRODUCTION

1.1 Background

Nuclear Medicine is the study and utilization of radioactive compounds in medicine to image and treat human disease. It relies on the tracer principle first espoused by Georg Karl Von Hevesy, in the early 1920s. The tracer principle is the study of the fate of compounds in vivo using a small amount of radioactive tracer which does not have any pharmacological response by the body to the tracer(Nuclear Medicine Physics:Handbook for teachers and students, IAEA 2014, p8).

These tracers are usually attached to chemical compounds that are attracted to specific organs bones or tissues, like iodine to the thyroid gland, MIBI or tetrofosmin to the heart. After being administered to the body, these must be a radionuclide. Special electronic instruments, such as scintillation or a gamma camera, which display these emissions into images, can detect these emissions (Helal, 2012).

The strength of nuclear medicine lies in using the tracer method to acquire information about how an organ is or is not functioning as it should. (Handbook for teachers and students, AIEA)

Myocardial perfusion imaging (MPI) with single photon emission computed tomography (SPECT) is a nuclear medicine imaging technique that uses gamma rays to scan the heart (Hendel et al, 2009).

It`s a well-established, highly standardized test to detect significant coronary artery disease and to risk-stratify patients with regard to cardiac event-free survival.

Myocardial perfusion single photon emission computed tomography(MPI-SPECT) has become essential for screening diabetic patient at high risk of silent myocardial ischemia.

The absorbed dose is a quantity that usually is estimated from the localized uptake and retention of administered radiopharmaceuticals, the radiation decay data of radionuclide and simulations of radiation transport in anthropomorphic models.

The absorbed radiation dose from internally deposited radionuclides is a major factor in assessing risk and therapeutic utility when evaluating new radiopharmaceuticals for use in nuclear medicine diagnostic or treatment. The measurement of the biodistribution of radiopharmaceuticals in human subjects to estimate radiation absorbed dose using the medical internal radiation dose (MIRD) schema. (MIRDPamphlet Nº16,Siegel et al, 2012)

The calculation of internal dose estimates is performed by summing the radiation absorbed in various target tissues from a number of source-organs in the body that contain significant quantities of radioactive material:

$D=(\tilde{A}/m)\ \Sigma\Delta_i\varphi_i$

Where D= dose in rad

$\tilde{A}$= cumulative activity

m= organ mass in grams

Δ_i= equilibrium dose constant in g.rad / uci-h

φi= absorbed fraction

To simplify calculations, the MIRD committee formed in the 1960s by the Society of Nuclear Medicine (SNM), introduced the s values which is the ratio effective absorbed energies by the organ weights of the standard man.

$\overline{D} = \tilde{A} * S$ where D= dose, Ã= cumulative activities and S= Mean absorbed doses.

1.2 STATEMENT OF THE PROBLEM

Clinical applications of nuclear medicine allow functional imaging of normal and abnormal tissues. Myocardial perfusion imaging is one of the purposes of SPECT imaging to examine the function of the heart muscle in order to diagnose ischemic diseases.

Following this principle that in stress situation the uptake of the diseased myocardium is less than the normal one. After injection of a radionuclide into the blood stream of the patient, SPECT imaging is performed first in stress situation; if there is an abnormality in the images, the same procedure will be repeated in rest situation within several days or within hours depending on the substance and pharmaceutical that are being used.

In Niger, with 16 million peoples, the prevalence of coronary artery disease was about 3% in2000 and probably higher than this in 2015. Because of this relatively high prevalence, the SPECT myocardial perfusion imaging becomes the second most requested scan after the bone scan in the nuclear medicine department of the Radio-Isotopes Institute of Niamey.

Whenever patients are exposed to ionizing radiation, an estimation of radiation doses is an essential element to balancing the risk and benefits of the proposed examination. During a Sestamibi myocardial perfusion, two injections are needed, 10 mCi during the maximum effort (stress) and 30 mCi for the rest scan.

The role of internal dosimetry in diagnostic nuclear medicine is thus to provide the basis for stochastic risk assessment. Once this risk is quantified, it may be used to optimize the amount of administered activity in order to maximize image quality while minimizing patient risk. This optimization process is important for pediatric patients owing to their enhanced organ radio sensitivities and years over which any stochastic effects may become manifest. The optimization should be considered, and always evaluated for any imaging procedure. (IAEA Report, 2011).

Accurate dosimetry of diagnostic procedures is important for making judgments on the diagnostic benefits to the patient compared to the associated radiation risks. Dosimetry of diagnostic radiopharmaceuticals is therefore primarily concerned with the dosimetry of the total population or group. The absorbed dose from internally distributed radioactivity used in diagnostic procedures is usually only calculated using models based on reference individuals and not specific patients. Accurate dosimetry for representative groups of patients for each specific investigation is needed in order to optimize use of the various alternative radio diagnostic techniques, and to estimate the collective radiation exposure and risk from nuclear medicine investigations (Hickson, 2011).

The current philosophy of radiation protection is based on the assumption that any radiation dose, no matter how small, may result in human health effects, such as cancer and hereditary genetic damage. But doses of ionization radiation less than 0.1Gy are critical for risk assessment of the general public, as well as of radiation

workers (Ahasanet al., 2004). Therefore, it is important to do research in the spectrum of the present work.

1.3 OBJECTIVES

To assess the radiation dose received by the patients undergoing SPECT myocardial perfusion imaging (MPI) with ^{99m}Tc-Sestamibi.

1.3.1. Specific Objectives

- To determine the cumulated activity in the heart, liver, kidneys and urinary bladder for patients undergoing MPI at various time after injection (10minutes,2h, and 4 h for heart, liver and kidneys and 10 minutes, 20 minutes and 2 hours for urinary bladder quantifications)
- To determine residence times (τ) of ^{99m}Tc-Sestamibiin the heart, liver, kidneys and urinary bladder;
- To determine the absorbed dose in the source-organs and target-organs of patients undergoing ^{99m}Tc-Sestamibi MPI using the OLINDA software.

1.4 RELEVANCE AND JUSTIFICATION

The results of internal dosimetry can be useful in estimating the amount of activity that can be administered to the patient and also serve as a way of comparing the risk to the benefits of these nuclear medical procedures with other modalities of diagnostic procedures (Alam*et al*, 2005).

The estimation of radiation dose can help to optimize image quality while using lowest radiation dose possible.

The performance of any diagnostic test requires a careful assessment of the risk and benefits of the test and optimization of protocols to minimize risks to patients, staff members, and the public. Procedures that utilize ionizing radiation should be performed in accordance with ALARA (As Low As Reasonably Achievable), Howard et al, 2011.

Absorbed dose from patients or any other radiation source depends on contact time, distance and intensity of radiation (Helal, 2012).

1.5 SCOPE AND LIMITATION

This study will assess the radiation dose to patients undergoing SPECT myocardial perfusion imaging at the Radio-Isotopes Institute, Abdou Moumouni University of Niamey – Niger.

The study will also estimate the cumulative activity10 minutes, 20 minutes, 2 hours, and 4 hours, after injection for patients undergoing ^{99m}Tc-Sestamibi SPECT-MPI.

The data collection will be done in Niamey-Niger at the Radio-Isotopes Institute of Abdou Mounouni University, and data analysis and data processing will take place in Accra at the School of Nuclear and Allied Sciences (SNAS).

1.6 ORGANISATION OF THESIS

This thesis is in a chronological order of five chapters. Chapter one is an introduction to the research and provides an overview of the current state of knowledge relevant to the study. Chapter two reviews existing literature relevant to the research problem. Chapter three focuses on the experimental and theoretical framework for the study. The results obtained are presented and discussed in chapter four. Chapter five contains the conclusions of the study and recommendations for further research.

CHAPTER TWO: LITERATURE REVIEW

In nuclear medicine applications, scintigraphic studies have been applied to different organs such as liver, spleen, heart, kidneys, bone, lung, thyroid, lymph glands etc. (UNSCEAR, 1993).

The procedures are using the administration of a small amount of radiopharmaceutical into human body in order to image organs. When radiopharmaceutical reaches the organ, the radiopharmaceutical is accumulated and released in particular ways. The accumulation of radiopharmaceutical will lead the organs to become radioactive and then, the others organs closer will received radiation dose internal dose from the source-organs (Hidayati 2013).

The absorbed dose levels for the critical organs are always high, during therapy. Although the absorbed dose levels of the critical organs during the nuclear medicine procedures are lower than those arising from therapy, their evaluation may be also considered important.

SPECT data from myocardial perfusion imaging (MPI) are normally displayed as a set of three slices orthogonal to the left ventricular (LV) long axis for both ECG-gated (GSPECT) and non-gated SPECT studies. The slices normally presented are horizontal long axis (HLA), vertical long axis (VLA) and short axis (SA) (N.DARVISH, 2013).

The cardiac scan is one of the most common scans in nuclear medicine. During the heart scan, among various organs, the kidneys and intestines absorb high amounts of radiopharmaceutical. Relation to high absorption fraction of Tc Sestamibi receiving by the bladder duringMPI and genital(ovaries and testes) organs are not yet

established. The ovaries are chosen as the critical organs, because they are the most radiosensitive organs for the genetic and somatic effects (Cember, 1992).

In order to know the risk and ensure the safety of human organs, it is necessary to know the amount of radiation dose absorbed by an organ (Alamet.al. 2005).

2.1 The basics of internal dosimetry

The absorbed radiation dose from internally deposited radionuclides is a major factor in assessing risk and therapeutic utility when evaluating new radiopharmaceuticals for use in nuclear medicine for diagnosis and/or treatment. Although direct measurements of absorbed dose and dose distributions in vivo would be preferable, this generally is not feasible for routine clinical studies. Absorbed dose, therefore, is a quantity that usually is estimated from the localized uptake and retention of administered radiopharmaceuticals, the radiation decay data of the radionuclide and simulation of radiation transport in anthropomorphic models (MIRD Pamphlet No.16). Dose estimates based on the generalized heart model of the revised MIRD Pamphlet No.5, are only a first approximation because there is no separation of heart walls from heart chambers, and it is unlikely that any radionuclide would be uniformly distributed throughout both walls and chambers.

The mean absorbed dose to an organ from an internally administered radiopharmaceutical is dependent on the characteristics of both the radionuclide and the pharmaceutical in terms of the type of radiation emitted and the spatial and temporal distribution of the radionuclide in the body. Internal dosimetry has been applied to the determination of tissue doses and related quantities for occupational exposures in radiation protection, environmental exposures in radiation epidemiology,

and diagnostic and therapeutic exposures in nuclear medicine (Zanzonico, 2000; Jönsson, 2007).

The mean absorbed dose, D (Gy) can be calculated using the MIRD formalism and the equation:

$$D = \tilde{A} * S \qquad (2.1)$$

Here, $\tilde{A}$ is the cumulated activity (MBq s), expressing the total number of decays during a particular time interval, and S is the mean absorbed dose to the target organ per unit cumulated activity in the source organ (Gy MBq^{-1} s^{-1}).

The S value thus takes into account all physical factors when calculating the energy absorbed by the target organ, from radiation emitted from the source organ. Practical applications may, however, introduce several uncertainties.

One such uncertainty is that the calculation of the mean absorbed dose is often based on the assumption that the radionuclide is uniformly distributed in the source volume. Also, human dosimetric models are based on an average size and age.

With regard to radiation protection purposes, the administration of radiopharmaceutical into human body needs to be assessed in order to consider the risk to the patients and the critical groups such as the family of patients, nurses and people who have contact with them (Helal, 2012). Moreover, the assessment might be useful for other purposes such as evaluation of clinical trials or internal dose assessment for new radiopharmaceuticals (Stabin et al, 1999).

One of the well-known radiopharmaceuticals for nuclear medicine procedure is technetium-99m. ^{99m}Tc Sestamibi previously has been used for myocardial perfusion studies (Joseph et al., 2003), but the application has been extended in scinti

mammography in breast cancer detection (O, 2010) and other sites such as thyroid (Perez-Monte, et al., 1996), brain tumors (Yokogami et al., 1998), and multiple myeloma (Pace, 2005).

For radiation protection purposes in diagnostic applications, human models are relevant in absorbed dose calculations because the purpose is to estimate the risk of late stochastic effects on a large population of patients undergoing the same type of examination. The use of dosimetry factors based on a standardized phantom and average-based biokinetics is thus justified. The discrepancy between the body geometry of the patient and that of the dosimetry model and the individual variation in time-activity biodistribution introduces inaccuracies into the absorbed dose calculation. However, these are less important when compared with the therapeutic situation.

When administering high activities for therapeutic purposes the aim is to produce sufficient deterministic effects on tumour cells but to avoid such effects on normal tissues. Therefore, the planning of radionuclide therapy is very important to ensure that the correct activity is administered to achieve the desired effect. The calculation of organ absorbed doses in patient-specific radionuclide therapy dose planning has to be as accurate as possible, and hence the errors and uncertainties in the models have to be reduced. Radionuclides emitting low-energy electrons, a non-uniform activity distribution within the organ or tissue can give large variations in the absorbed dose to different cells or areas in the organ (Jönsson, 2007). Studies have shown that the dose absorbed by radiolabeled Kupffer cells after ^{99m}Tc-sulfur colloid injection was approximately 15,000 times the mean electron dose to the same cells as estimated using the conventional MIRD Schema (Robinson, 1997). This illustrates the importance of developing small-scale anatomy models for more accurate internal

dosimetry. In patient-specific dosimetry, both a patient-specific physical model as well as patient-specific biokinetic data should be included. If the inhomogeneous activity distribution within an organ or tissue could also be accounted for, the accuracy in the absorbed dose calculation would increase (Jönsson, 2007).

2.1.1 Radiation dose assessment

In any use of ionizing radiation, an analysis of the risk and benefits is needed to justify and optimize the procedures involved. When radiopharmaceuticals are administered to patients to diagnose and evaluate disease or for therapeutic purposes, estimates of radiation does to major organs and tissues of the body are required. Internal dose estimates are performed via calculations and the use of theoretical models, as it is not possible to make direct measurements of the radiation doses received. Standardized models of human body and standardized models of radiopharmaceutical behavior in the body may be used tocharacterize the radiation doses received by various tissues in the body (Stabin, 2007).

Dose calculations

To estimate absorbed dose in a given organ of the body, one must determine the amount of energy deposited per unit mass of the organ. This yields the quantity absorbed dose, when expressed in proper units, and can be extended to calculation of equivalent and effective dose if desired. A generic equation can be developed to estimate the absorbed dose rate in an organ by assigning numerical values to all quantities needed to establish the energy deposited dose rate in the organ. Once the

radionuclideis involved, the energies and abundances of the nuclideare known. When the cumulative activity is estimated, the absorbed dose within the organ is known: This quantity is most often called the absorbed fraction.

The clinical use of internal dosimetry in Nuclear Medicine

The clinical uses are:

1- To estimate the absorbed dose received for patients undergoing diagnostic nuclear medicine procedures;

2- To plan patient treatments by using tracer doses;

3- Treatment optimization in multiple cycles treatments or in combined use of radionuclide therapy and external radiotherapy;

4- Clinical evaluation of new radiopharceuticals.

Standard dose equations

A generic equation for the absorbed dose rate in an object uniformly contaminated with radioactivity (for example an organ or tissue with radiopharmaceutical uptake) may be shown as:

$$D = \frac{k\,\tilde{A}\sum_i n_i E_i \phi_i}{m} \quad (2.2)$$

D = absorbed dose in a target organ (rad or Gy)

Ã = cumulated activity (sum of all nuclear transitions that occurred) in a source organ (μCi-hr or MBq-s)

n = number of radiations with energy E emitted per nuclear transition

E = energy per radiation (MeV)

ϕ = absorbed fraction (fraction of radiation energy absorbed in the target)

m = mass of target region (g or kg)

k = proportionality constant (rad-g/μCi-hr-MeV or Gy-kg/MBq-sec-MeV)

An example calculation of k is shown here, to obtain dose in rad from activity in μCi, with mass in g, and energy in MeV:

$$k = \frac{3.7x10^4\, dis}{s-\mu Ci}\,\frac{3600\, s}{h}\,\frac{1.6x10^{-6}\, erg}{MeV}\,\frac{g-rad}{100\, erg} = 2.13 \quad (2.3)$$

In general, internal dose can be calculated by the following simple equation: $D = N \times DF$ where N is the number of nuclear transitions that occur in source region S, and DF is a "dose factor". The factor DF contains the various components shown in the formulas for S and SEE (Specific Effective Energy) basically it depends on combining decay data with absorbed fractions(AFs), which are derived generally using Monte Carlo simulation of radiation transport in models of the body and its internal structures (organs, tumors, etc.):

$$DF = \frac{k\sum_i n_i E_i \phi_i}{m} \quad (2.4)$$

When the components of the various published internal dose calculation schemes are carefully studied, they can all be reduced to this single generic equation:

$$D = \tilde{A} \cdot S = A_0 \cdot \tau \cdot S \quad (2.5)$$

where Ã is defined as cumulated activity, τ is the residence time, which is simply equal to $\tilde{A}/A_0$, the cumulated activity divided by the patient's administered activity (A_0), and S is given by:

$$S = \frac{k\sum_i n_i E_i \phi_i}{m} \qquad (2.6)$$

Time-activity functions are usually given in the form of one or more exponential functions. The function may describe only the biological clearance of the agent (and thus be associated with a biological half-life) or the biological clearance and the radioactive decay (and thus be associated with an effective half-life). The relationship between biological half-life, T_b, physical half-life, T_p, and effective half-life, T_e, is given as:

$$T_e = \frac{T_b \times T_p}{T_b + T_p} \qquad (2.7)$$

For a compound whose clearance may be described by a single exponential term:

$$\tilde{A} = \int_0^\infty A(t)\,dt = \int_0^\infty f\ A_o e^{-\lambda_e t}\,dt = \frac{f\ A_o}{\lambda_e} = 1.443\ f\ A_o T_e \qquad (2.8)$$

Where: f = fraction of administered activity taken up

A_0 = activity administered (e.g. μCi)

T_e = effective half-life (e.g. h)

Ã = cumulated activity (e.gμCi-h)

If more than one exponential term is needed to describe the clearance, we will simply have a repetition of this expression, with different values of f and T_e for each term.

In the International Commission on Radiological Protection (ICRP) system of radiation protection for workers (ICRP 1979), the dose equation is: $H = U_S \cdot SEE$

Here, H is the dose equivalent (the absorbed dose, D multiplied by a radiation weighting factor w_R, formerly known as a quality factor (Q), U_S is the number of nuclear transitions that occur in source region S, and SEE is:

$$SEE = \frac{k\sum_i n_i E_i \phi_i w_{R_i}}{m} \qquad (2.9)$$

As written, the equations above give only the dose from one source region to one target region, but they can be generalized easily to multiple source and target regions. Since the factor N is analogous to Ã and U_S, and the factor DF is analogous to S and SEE, the MIRD and ICRP systems of dose calculation can be accommodated by the equation D = N x DF, whose terms are more intuitively understandable by most users. The MIRD concept of "residence time" (Loevinger, 1988) has often caused confusion, because of its apparent units of time (even though it really expresses the number of nuclear transitions that occur in a source region) and because of the use of this term to represent the "mean life" of atoms in biological or engineering applications (Stabin, 2007; Islam, 2011).

2.1.2 Evolution of Dosimetric Formalisms

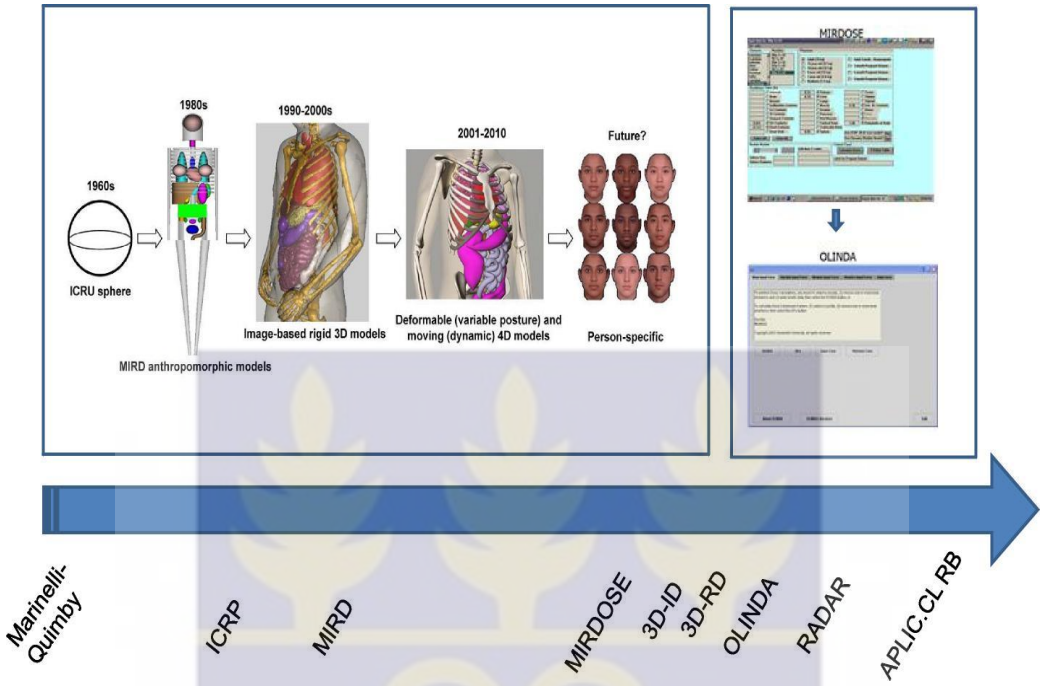

Figure 2.1: Evolution of dosimetric formalism

The current generation of anthropomorphic phantoms began with the development of the Fisher-Snyder phantom, which employed a combination of geometric shapes - spheres, cylinders, cones, etc. to create a reasonably accurate representation of the body.

Monte Carlo computer programs were used to simulate the creation and transport of photons through these various structures in the body, which's atomic

compositions and densities were based on data provided by the International Commission on Radiological Protection (ICRP103) in its widely quoted report on "Reference Man", now updated in a more recent report (ICRP103). These reports provide various anatomical data helpful in producing dose calculations for standardized individual, (Bolchet al., 1998). Absorbed fractions and dose conversion factors (S values), as defined above, for over 100 radionuclides and over 20 source

and target regions, were also published (Synder, 1978). Absorbed fractions for photons at discrete energies were published for these phantoms, which contained approximately 25 source and target regions. Tables of S values were never published, but ultimately were made available in the computer software called "MIRDOSE" (Stabin, 1996), which was widely used by the nuclear medicine community.

Stabin et al. developed a series of phantoms for the adult female, including a model of the non-pregnant adult female and the woman at three stages of pregnancy. These phantoms modeled the changes to the uterus, intestines, bladder, and other organs that occur during pregnancy, and included specific models for the fetus, fetal soft tissue, fetal skeleton, and placenta. S values for these phantoms were also made available to the dosimetry community through the MIRDOSE software.

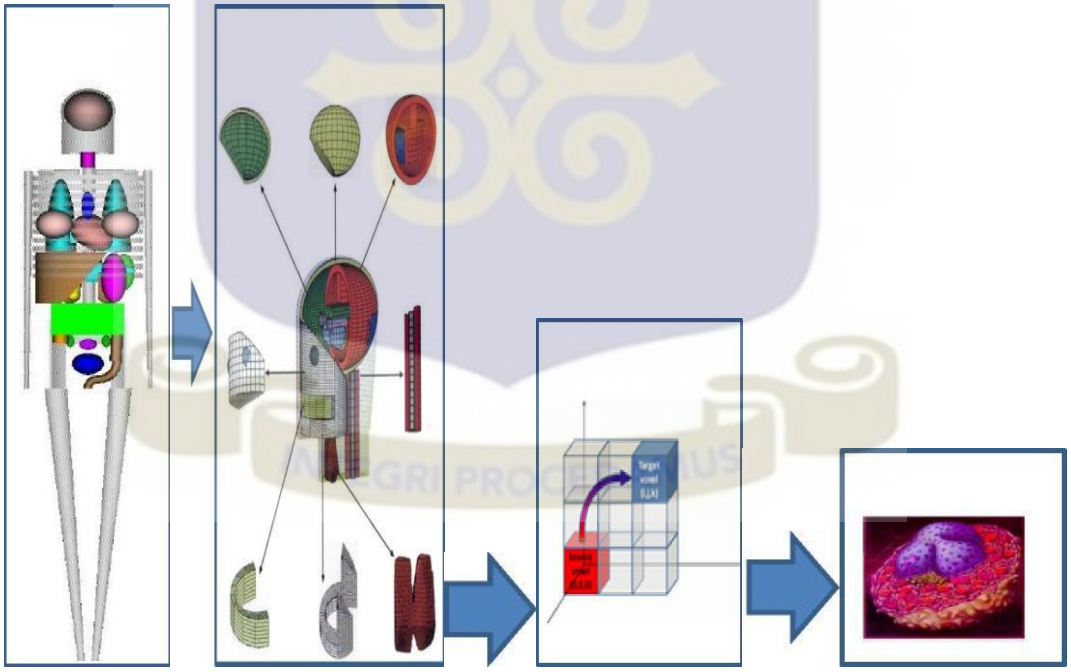

Figure 2.2: S-values phantoms through MIRDOSE software

A number of authors have developed more realistic phantom using image methods to replace the stylized models of the 1970`s with voxel-based (A) or mathematical methods like non-uniform rational, (Bolchet al., 2013.).

2.1.3 Planar methods for quantification

In the introduction to MIRD Pamphlet No. 16 (Siegel et al, 1999), the following is stated:

To determine the activity-time profile of the radioactivity in source regions, four questions need to be answered.

1. What regions are source regions?
2. How fast does the radioactivity accumulate in these source regions?
3. How long does the activity remain in the source regions?
4. How much activity is in the source regions?

The first question concerns identification of the source regions, whereas the second and the third questions relate to the appropriate number of measurements to be made in the source regions, as well as the timing of these measurements. The fourth question is addressed through quantitative external counting and /or sampling of tissues and excreta.

Each source region must be identified and its uptake and retention of activity as a function of time must be determined. This provides the data required to calculate cumulated activity or residence time in all source regions.

The remainder of the body is the total body minus the source regions and must be considered as a potential source as well. Mathematical models that describe the kinetic processes of a particular agent may be used to predict its behavior in regions where direct measurements are not possible, but where sufficient independent knowledge about the physiology of the region is available to specify its interrelationship with the regions or tissues whose uptake and retention can be measured directly. The statistical foundation of a data acquisition protocol designed for dosimetry requires an adequate number of data points and careful selection of the timing of these points. As the number of measurements increases, the confidence in the fit to the data and in the estimates of unknown parameters in the model is improved. As a heuristic or general rule of thumb, at least as many data points as the number of initially unknown variables in the mathematical curve-fitting function(s) or in the compartmental model applied to the data set, should be obtained. For example, each exponential term in a multiexponential curve-fitting function requires two data points to be adequately characterized. On the other hand, if it is known a priori that the activity retention in a region can be accurately represented by a monoexponential function, restrictions on sampling times are less stringent as long as enough data points are obtained to derive the fitted function. Because of problems inherent in the collection of patient data (e.g., patient motion, loss of specimen, etc), the collection of data above the necessary minimum is advisable."

Image Quantification

Nuclear medicine images can be used for either detection tasks, such as identifying perfusion defects, or quantitative tasks, such as estimating ejection fraction, standardized uptake values (SUVs) or organ absorbed dose. Obtaining images that are suitable for quantitative tasks often requires additional processing compared with

those used for visual interpretation. This additional processing often results in improved resolution and contrast and reduced artefacts. These improvements in the image will often, but not always, translate directly to improved performance on detection tasks. For example, the development of attenuation correction methods for cardiac SPECT has improved detection of myocardial perfusion defects, while at the same time providing images which are quantitatively more accurate.

For image quantification, data are collected with a nuclear medicine gamma camera. Quantification of data gathered with these cameras may be achieved in a number of ways. One method is the use of developed and processed anterior and posterior projection images of the patient with the conjugate view method. As this is a projection image, the actual depth of objects containing activity within the patient is not known. Region of interest (ROIs) are drawn around objects that are recognizable as internal organs or structures; the number of counts in a ROI, however, cannot be used directly to calculate how much activity is in the organ. Some corrections are needed to the observed number of counts to obtain a reliable estimate of activity in this object. In this method, images are taken in front of and behind the patient, and a geometric mean of the two values is taken. This geometric mean, when corrected for attenuation, is theoretically independent of depth for most radionuclides of interest, and thus this quantity is thought to be the most reliable for use in quantification. Corrections for the presence of scattered radiations within the photopeak channel can be addressed by using an appropriate scatter correction technique (Stabin, 2010). In this method, the source activity Aj is given by the expression 2.10 (JM Pereira *et al*, 2010):

$$A_j = \sqrt{\frac{I_A I_P}{e^{-\mu_e t}}} \frac{f_i}{C} \qquad (2.10)$$

$$f_j = \frac{(\mu_j t_j / 2)}{\sinh(\mu_j t_j / 2)} \qquad (2.11)$$

where I_A and I_P are the observed counts in the anterior and posterior projections (counts/time), t is the overall patient thickness, μe is the effective linear attenuation coefficient, C is system calibration factor C (count rate per unit activity), and the factor f (equation 2.11) represents a correction for the source region attenuation coefficient (μj) and source thickness (tj) (i.e., source self-attenuation correction). This expression assumes that the views are perfectly collimated (i.e. they are oriented towards each other without offset) under the model of narrow beam geometry without significant scattered radiation effects. Corrections for scatter are usually necessary, and a number of methods have been proposed (Siegel et al, 1999, Jönsson, 2007; Stabin, 2008; Gahrouei, 2012).

Corrections for Scattered Radiation

Scattering of the gamma-rays in the patient not only creates widening of the measured 140 keV energy spectrum. Apart from scattering in the body, scatter can also occur in the collimator and detector system. Both types of scatter cause deterioration of image resolution. Scatter correction can be solved by using either multiple energy windows on the measured ^{99m}Tc spectrum to determine the scatter component in the signal empirically (Bucerius et al., 2012).

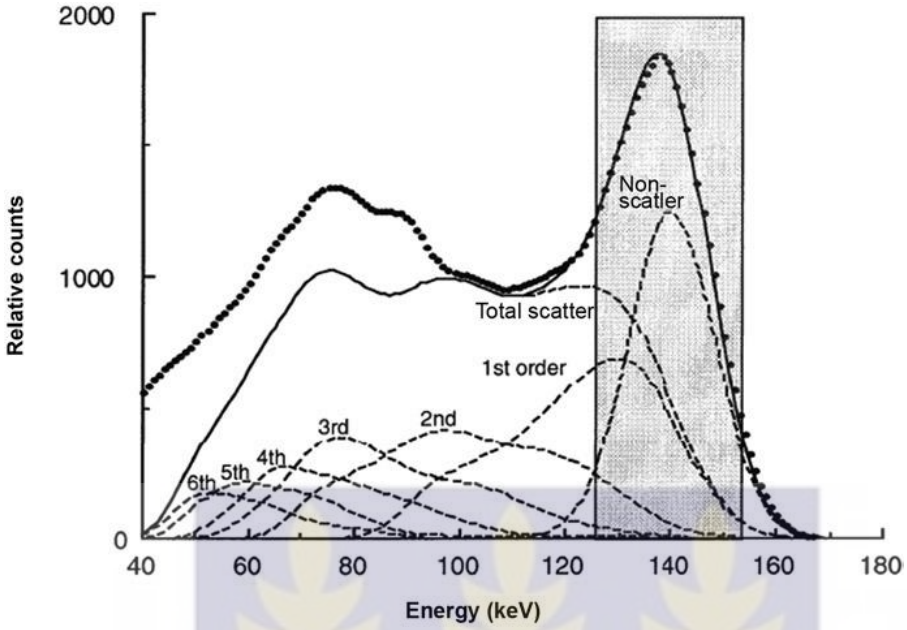

Figure 2.3: Energy spectrum for the 140 keV 99m-Tc

One relatively straightforward correction procedure for scatter compensation involves establishing adjacent windows on either side of the photopeak window, with the area of the two similar adjacent windows equal to that of the photopeak. The corrected (true) photopeak counts C_T are given by the expression:

$$C_T = C_{pp} - F_S * (C_{LS} + C_{US}) \qquad (2.12)$$

Where C_{pp} is the total count recorded within the photopeak window, while C_{LS} and C_{US} are the counts within the lower and upper scatter windows, respectively. If the areas of the scatter windows are not equal (in sum) to that of the photopeak window, then an appropriate scaling factor (F_S) should be applied. Subtraction of the adjacent windows is assumed to compensate for the high-energy photon scatter tail upon which the true photopeak events are superimposed. Even if the areas of the scatter windows are equal to that of the photopeak window, use of a scaling factor other than unity may provide the best correction for scatter in a given system with a particular

radionuclide. This may be determined by the study of a known volume source in a water phantom whose dimensions are similar to that of a human subject (Stabin, 2007, 2008). Other corrections are often required as well.

Corrections for Background Activity

Background correction in planar images, was performed as:

$$C = C_{ROI\ SOURCE} - C_{ROI\ Background} \times S_{source} \quad (2.13)$$

Where C gives the corrected counts in the region of interest in the source area, $C_{ROI\ Source}$ is the number of the counts in the source region of interest, $C_{ROI\ background}$ is the mean value of the counts/ pixel in a background region drawn close to the source and S_{source} is the source area in pixels. The subtraction was performed for each projection, Ia and Ip, before application of equation 2.10. Equation 2.10 was used to estimate the activity in a drawn ROI, performing attenuation correction on the whole ROI. On some images background ROIs were also drawn far from the source area, to evaluate the effect of variability in the placement of background ROIs.

For SPECT images, background subtraction was performed using equation 2.13 as well. It was done to compensate the contribution of spurious numerical values that appear in all regions of the images after reconstruction and to compensate for background spill-in from the surround neighboring into the source area (Zingerman et al.2009).

Other study presented a method that takes into account the thickness of the organ and the background volumes above and below the organ, and the method also includes effects of different attenuation coefficients in different layers in the region of interest.

A simplified method was proposed by Buijs et al, 1998, in which only the organ thickness, *l*, and body thickness, *L*, are required. Here, the fraction of the total background activity, *F*, is calculated using equation 2.14:

$$F = 1 - (l / L) \qquad (2.14)$$

The method proposed by Buijs et al. is accurate but is more sensitive to low organ-to-background activity concentration ratios (Jönsson**,** 2007; Stabin, 2007, 2008).

Correction for Overlapping Organs and Regions

It is not uncommon for some organs or tumors to have overlapping regions on projection images. The right kidney and liver are frequently partially superimposed on such images, as are the left kidney and spleen, for example. When organ overlap occurs, an estimate of the total activity within a source can be obtained by a number of approximate methods. For paired organs, such as kidneys and lungs, one approach is to simply quantify the activity in one of the organs for which there is no overlap with other organs, and multiply the number of counts in this organ by two to obtain the total counts in both organs. Another approach is to draw a ROI over the organ region in scans where there is overlap, count the number of pixels and note the average count rate per pixel, then use a ROI from another image in which there is no apparent overlap and the whole organ is clearly visible; count the number of pixels in a larger ROI drawn on this image, and then multiply the count rate per pixel from the first image by the number of pixels in the second image. Or, equivalently, take the total number of counts in the first image and multiply by the ratio of the number of pixels in the second to the first image ROIs. If a significant overlap of images with

another organ is not possible, an approximate ROI may need to be drawn just from the knowledge of the typical shapes of such organs. This kind of approximation is obviously not ideal, but may be necessary.

In addition, calibration coefficients for each radionuclide and gamma camera/collimator combination must be obtained by imaging a small source of known activity for a fixed amount of time. The attenuation characteristics of the camera may be studied by imaging this source with various known thicknesses of tissue equivalent material interposed between the source and camera, and fitting the results (counts versus thickness) to an exponential function (Jönsson, 2007; Stabin, 2007; Siegel et al, 1999).

2.1.4 Quantification of tomographic data

Tomographic imaging offers the potential for improved dosimetric accuracy due to its increased contrast when compared with planar imaging.

Tomographic data are particularly useful for dosimetry where there is suspected heterogeneous uptake of activity in the source organ or underlying or overlying background activity. To date, Positron Emission Tomography (PET) data have been little used for dosimetry, although PET quantification is an active area of research in its own right. Standardized uptake values (SUVs) are used to quantify radiotracer uptake and, whilst prone to some uncertainty, are nevertheless used clinically with more regularity than quantification of SPECT or planar data. SUVs are defined as

$$SUV = \frac{\text{tracer activity concentration in tissue}}{\text{injected tracer activity/ patient weight}} \qquad (2.15)$$

Quantification of image data has been considered for many years, although as yet there are no standardized methods for quantifying SPECT or PET data. This remains the largest single obstacle to accurate dosimetry, and is currently a strong focus of research. It is probable that this task will be made easier with the advent of dual modality scanners and it is hoped that in time manufacturers will develop systems that are adapted to high energy high activity imaging, whereby camera sensitivity may be sacrificed to some extent in favour of spatial and energy resolution (Stabin, 2007; Siegel et al, 1999).

2.2 Radiopharmaceuticals

A radiopharmaceutical is a radioactive compound used for the diagnosis and/or treatment of diseases. Most radiopharmaceuticals are for diagnostic purposes, only about 5% are used for therapy. Because most radiopharmaceuticals are administered by intravenous administration, they should be sterile and non-pyrogenic.

2.2.1 Uncertainty of Biokinetic Model of Radiopharmaceuticals

Uncertainty analysis is the computation of the total uncertainty induced in the output by quantified uncertainty in the inputs and models, and the attributes of the relative importance of the input uncertainties in terms of their contributions, whereas sensitivity analysis is the computations of the effect of changes in input values or assumptions, including boundaries and model functional form, on the inputs. The following five steps were including in the analysis:

1- Uncertainty of input: The source of uncertainty of model parameters were carefully analyzed and evaluated;

2- Sampling: Sampling techniques are needed to generate samples of the model inputs parameters(variables);

3- Modelling: To predict the kinetics and retentions of radiopharmaceutical in humans, biokinetics modelling is required;

4- Uncertainty of output: Model predictions for different organs and tissues at different time periods resulted in huge amounts of data;

5- Sensitivity of parameters: in order to identify the most influential parameter in the model, the concepts of the standardized rank regression coefficient (SRRC) and the partial rank correlation coefficient (PRCC) were used. The SRRC can be computed by constructing regression models, which approximate the rank transformations of the sampled model input and output variables. The PRCC measures the rank correlation between one defined output variable with an input variable, under the condition that the indirect influence on this defined output variable due to other further input variables in somehow eliminated, (Li et al, 2010).

2.2.2 Radiopharmaceuticals used in diagnostic imaging procedures

Scintigraphic imaging procedures produce images that represent the distribution of a radiopharmaceutical within a patient or phantom. A radiopharmaceutical consists of two components. The first component is a photon emitting radionuclide and the second is the pharmaceutical compound. The photons emitted from the radionuclide

are used for imaging while the pharmaceutical compound dictates the distribution within a patient.

Several factors must be taken into consideration when selecting a radionuclide to be used in nuclear medicine imaging. Among these factors are the type of radiation the radionuclide emits, the energy of the emitted radiation, the radionuclide's half-life, and its ability to form a stable bond with the pharmaceutical compound.

First, the type of radiation must be photon radiation. Alpha and beta radiation are particles, which deposit their energy locally and as a result, have a short range in tissue.

This type of radiation significantly contributes to the dose received by the patient and not to the formation of an image. In contrast, photons with appropriate energies may pass through several centimeters of human tissue before being absorbed. This increases the number of photons emitted that reach a detector, and reduces the radiation dose to the patients.

Second, the energy of the radiation is important consideration as there is a limited range of energies able to be detected reliably by current imaging equipment. The energies of diagnostically useful photons lie in the range of 70 to 200 keV. Photon radiation with energy lower than 70 keV will generally not escapefrom the patient and therefore contribute to the dose. Photons with energies higher than 200 keV can penetrate the septa of the collimator to produce artifacts in the image, or pass through the NaI(Tl) crystal without interacting and detrimentally affect the counting statistics. Medium and high-energy collimators can overcome these problems but these suffer from reduced spatial resolution and sensitivity compared to low energy collimators (Gurk, 2007).

Third, the half-life of the radionuclide must be considered. There are two components of half –life, physical and biological. The physical half-life is unique to the radionuclide and determines how the activity changes with time. The biological half-life is based on how long the radiopharmaceutical will be present in the organ of interest. This is described by the uptake and clearance rate of each organ and is dependent on the organs function. This is also known as the kinetics of the radiopharmaceutical. Together, the physical and biological half-lives determine how long the radiopharmaceutical is present in the body and thus how much dose the patient receives. As such, the radionuclide should be chosen with a physical half-life that ensures enough activity is present at the time of a scan to form an image, but which also decays away expeditiously to ensure the radiation does not significantly contribute to patient dose after the imaging procedure is completed.

The final consideration in radionuclide selection is that it should form a strong bond with its pharmaceutical compound. This ensures the photon emitting radionuclide is distributed to and within the intended organ or organs under investigation. A nuclear medicine imaging procedure becomes worthless if the radionuclide and pharmaceutical have separated at the time of imaging.

Several different radiopharmaceuticals have been used in recent years for cardiac imaging in nuclear medicine and the dosimetry of these agents may be quite different. The dosimetry of radiopharmaceuticals currently used in nuclear cardiology is reviewed, and uncertainties in the dose are discussed. Relative radiation risks for these radiopharmaceuticals also are discussed.

Various radiopharmaceuticals are used for SPECT myocardial perfusion and their respective radiation risks are below.

^{201}Tl-Chloride (half-life= 72.9 h), administered as an intravenous bolus injection, has been used for several decades to image the myocardium. The uptake of ^{201}Tl-chloride by organs such as the liver, kidneys, heart and intestines varied widely.

^{99m}Tc-MIBI (Methoxy isobutyl isonitile), (^{99m}Tc half-life = 6.02 h), known also as Sestamibi, is a cationic compound used in studies of cardiac ventricular function and myocardial perfusion. The clearance from blood is rapid; uptake is high in the muscle, liver and kidney and is lower in the thyroid and salivary glands.

^{99m}Tc-Tetrofosmin is a lipophilic technetium phosphine dioxo cation (trade name Myoview) is used study myocardial perfusion. It is cleared rapidly from blood and shows marked uptake in the liver, muscle, heart wall, kidneys and salivary glands.

^{99m}Tc-labeled Red Blood Cells (RBCs) circulate in the bloodstream and are useful in the evaluation of cardiac function. They are cleared from the body with biologic half-times of 40-80 h, and some urinary activity is detectable.

Technetium 99m characteristics

The Tc-99m radionuclide emits 140.5 keV photons. These photons are attenuated 50% in a thickness of 4.6 cm of human tissue and are therefore able to escape the patient and be detected. Second, the physical half-life of Tc-99m is 6.02 hours. This ensures that patient dose is kept to a reasonable level. The method of producing Tc-99m is also straightforward. The Mo-99 nucleus undergoes β- decay:

$$^{99}Mo \rightarrow {}^{99m}Tc + e^{-} + \bar{\nu}$$

Mo-99m generators or 'cows' are usually delivered to a hospital at the beginning of a week. Staff then 'milks' the generator by washing the internal column with saline to produce the sodium pertechnetate complex ($Na^{99m}TcO_4$). This technetium ion is then

attached to a pharmaceutical appropriate to the organ of interest. For these reasons, Tc-99m is used in 85-90% of all nuclear medicine scans, (Gurk, 2007).

Table 2.1 Standard Myocardial perfusion SPECT patient radiation doses:

Study	Injected activity	Effective dose estimâtes
1-day rest/stress 99mTc-Sestamibi	10 mCi for rest 30 mCi for stress	11.4 mSv
2-days stress / rest or rest /stress 99mTc-Sestamibi	25 mCi stress 25 mCi rest	14.8 mSv
Stress-only 99mTc-Sestamibi	25 mCi stress	6.8 mSv

(Gordon et al, 2012)

2.3. Indications for Myocardial perfusion Imaging (MPI).

Myocardial Perfusion Imaging is a nuclear medicine technique to examine the heart muscle(N.DARVISH, 2013). The test is used to:

• Diagnose coronary artery disease (CAD) and various cardiac abnormalities such as myocardial infarction and atheromatous plaques.

• Identify how critical is the stage of CAD and locates the coronary stenosis in patients.

• Prognosticate or define the degree of risk in patients who are at risk of having CAD e.g. myocardial infarction abnormalities.

• Check if the patient is in good condition after bypass graft and angioplasty.

2.4 Image acquisition

Instrumentation

A single or double headed gamma camera equipped with a low-energy, high-resolution collimator is used for myocardial perfusion technetium-99m based. A 15% energy window: (±5%), centered over the 140-keV photopeak of technetium-99m should be set.

The acquisition parameters

- Low energy High Resolution (LEHR);
- Acquisition matrix: 128 × 128;
- 1.43 zoom;
- 32 images acquired 30 seconds each;
- Rotation mode of the head of the gamma camera: non-circular 180 ° (Starting from -45 to 135 °).
- First acquisition, post stress is made 30 to 40 minutes after injection of the radiotracer.
- Second acquisition at rest is done 3-4 hours after the first if using one day protocol (only in patients with abnormal or suspicious acquisition post stress).

2.4.3 SPECT Imaging

Basic principle

SPECT Imaging is a technique that uses a gamma camera to trace gamma rays; gamma emitting radioisotope (radionuclide) is injected intravenously into the patient. The chemical process that allows the marking is as follows(Darvish, 2013);

⇨the radioisotope is attached to a specific ligand to obtain a radioligand

⇨Radioligand that bind to certain types of tissues

⇨The combination of ligand and the radioisotope are carried and bound to the place of interest in the body

⇨Thus the place is marked and can be seen due to the gamma emission of isotope.

Image reconstruction

Image reconstruction for SPECT can be done either by filtered back-projection or by iterative methods. Filtered back-projection for SPECT is identical to the one performed in CT which is used for acquiring view set for slices and reconstructing the corresponding image. Every sample in the views is the sum of the image values passed by the rays (Smith, 1997).

In mathematical aspect, image reconstruction from a series of projections can be done by using inverse Radon transform.

Filtered Back-projection Techniques

The signal is produced along parallel X-rays. Hence the data can be filtered and back projected to obtain the image.

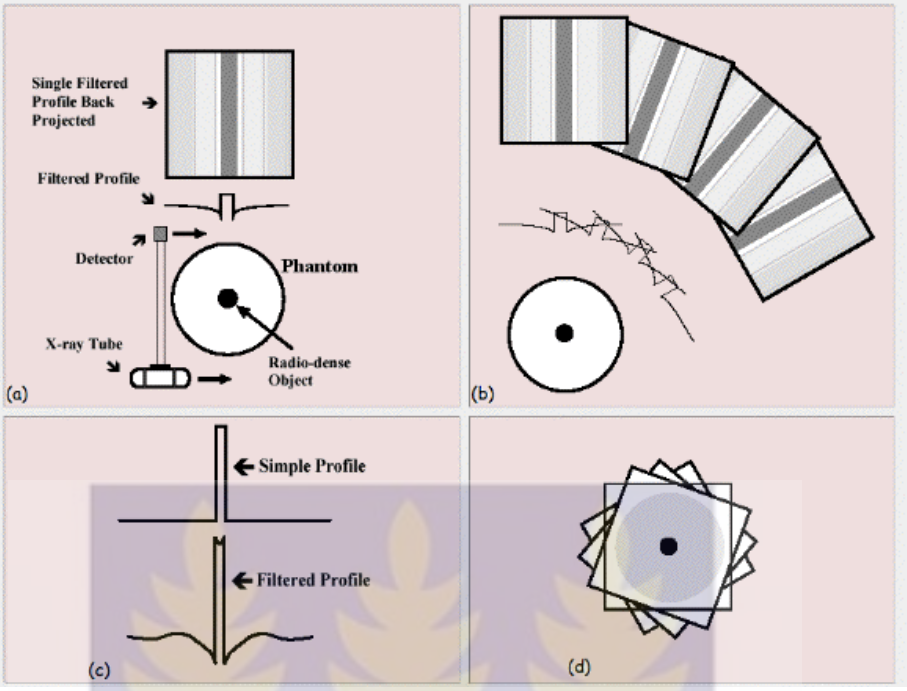

Figure 2.4: Filtered back projection: The views are filtered before back projection during the reconstruction of image. In mathematical basis, the end result is more accurate. This algorithm is the most commonly used algorithm when it comes to CT systems(Darvish, 2013).

.

Attenuation correction

The gamma rays coming from the radiotracers that are placed in the Centre of the body have more attenuation than the radiotracers that are placed close to the surface since they have to pass through more tissues. Consequently, attenuation correction is needed for a proper quantitation. In order to achieve this objective, an attenuation map is generated due to the density difference throughout the body. For more attenuated regions, photon counts are added back to that region. On the other hand counts are

subtracted from less attenuated regions to obtain a properly defined data. (DARVISH, 2013).

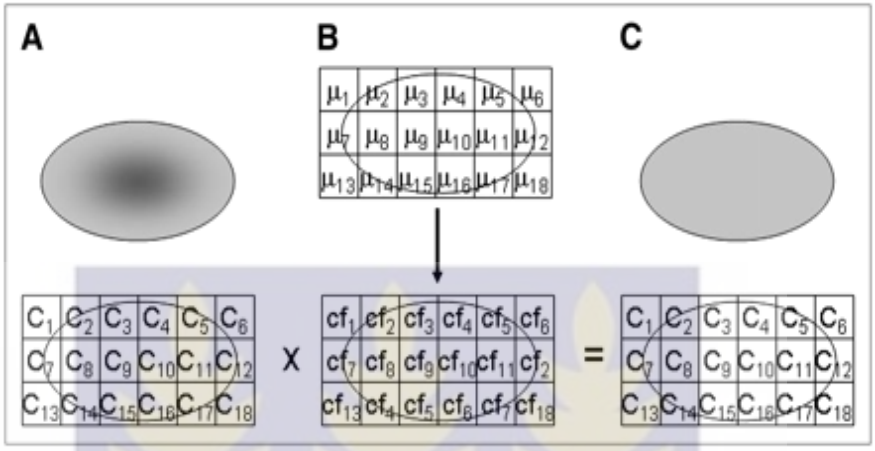

Figure 2.5: Attenuation correction

a) Uncorrected SPECT image of a material consisting of uniform radioactivity. The dark area is due to attenuation as the gamma rays pass through the material. b) Correction factor map with low scaling factor near the surface and high scaling factor at the Centre c) Initial image is multiplied by the attenuation factors and the uniform distribution is obtained more accurately.

CHAPTER THREE: MATERIALS AND METHOD

This chapter presents the materials used to performthis research work and the method used toarrive at the results. The materials include the equipment and software used for the study.

3.1 Equipment and software

The equipment used to perform myocardial perfusion imaging for this study is the Mediso gamma cameradouble heads. The system is connected to a computer which displays acquired images using InterViewXP® software. The InterViewXP® softwareenables thedrawing ofthe regions of interest (ROIs) to demarcate organs being studied. The thicknesses of the organs in anterior and posterior positions were measured by scanning patient with a CT systemHitachi supra 16 slices. Dose calculations were performed with MATLAB and OLINDAsoftware. The conjugate view method was used to estimate the average activity in the organsat different times by using the Microsoft Excel 2010.

3.1.1 The Mediso gamma camera system

The Mediso gammacameraof the Nuclear Medicine department, Radioisotopes Institutein Niger was used to perform ^{99m}Tc-Sestamibi whole-body scans in this study. The gamma camera contains 59 photomultiplier-tubes (PMT) characterized by improved energy resolution, shielding and long-term stability. The thallium-doped sodium iodide crystal size is 585mm×470mm with 9.5mm thickness. The proper positioning of the gantry, patient bed and table highly impacts image quality. Access

to the standard gantry controls is provided on the acquisition screen andthe user can easily adjust the positioning of the gantry and patient prior to imaging.

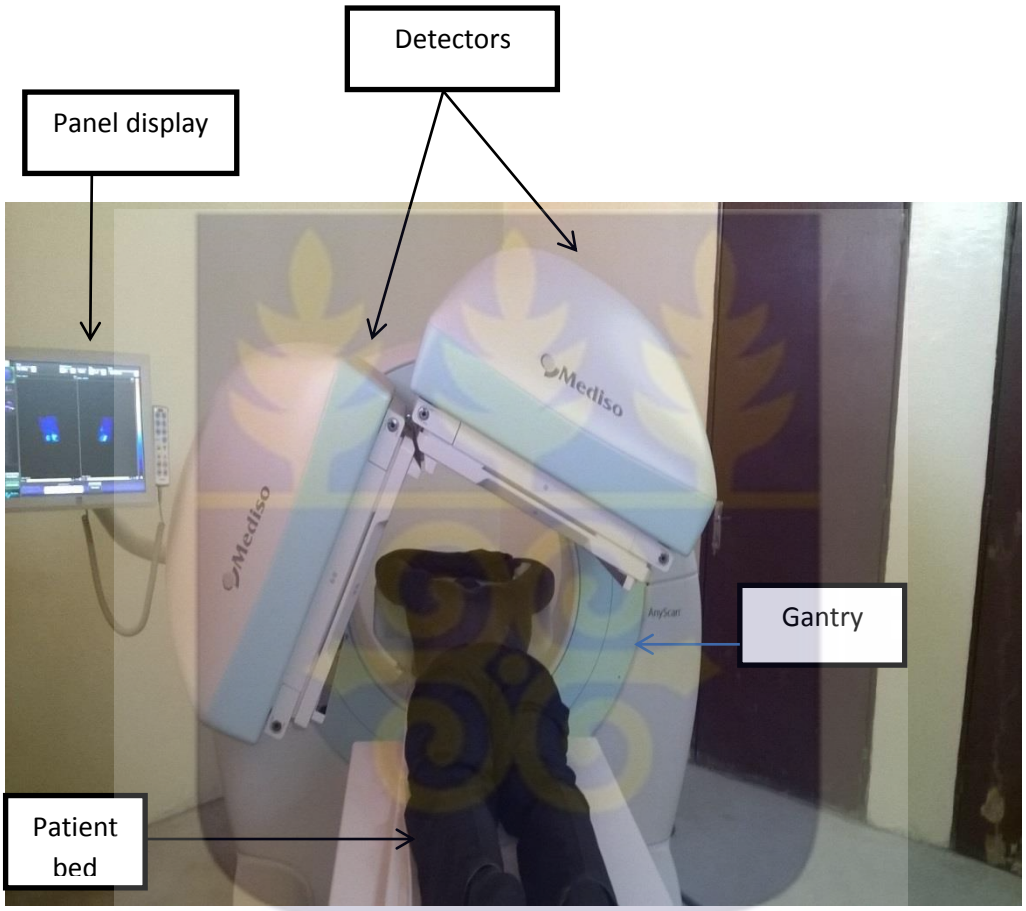

Figure 3.1: Mediso gamma camera

3.1.2 The InterViewXP®software

The InterViewXP® application is designed so that many of the display (display tools toolbar, color bar, cine, and curve tools) and processing features (filter tool and ROI tool) are common to all activities that are needed to display raw and processed data. In this work, the ROI tool was used to get the counts of activity of different organs such as heart, liver, kidneys and bladder.

Drawing of regions of interest (ROI)

Region of interest

ROI selection

- **"Heart"** ROI is needed for"**RBF/CO%", "Patlak"** and **"Deconvolution"** calculations.Mostgamma camera images do not visualize the heart, so heart ROI is drawn on the aorta.Liver ROI is needed for deconvolution. Liver ROI is needed to sign a representative territory of liver, because most of images do not contains the full liver. Kidney ROIs are needed for relative kidney and relative patlak calculations and bladder ROI is needed for reflux and bladder curve calculation.

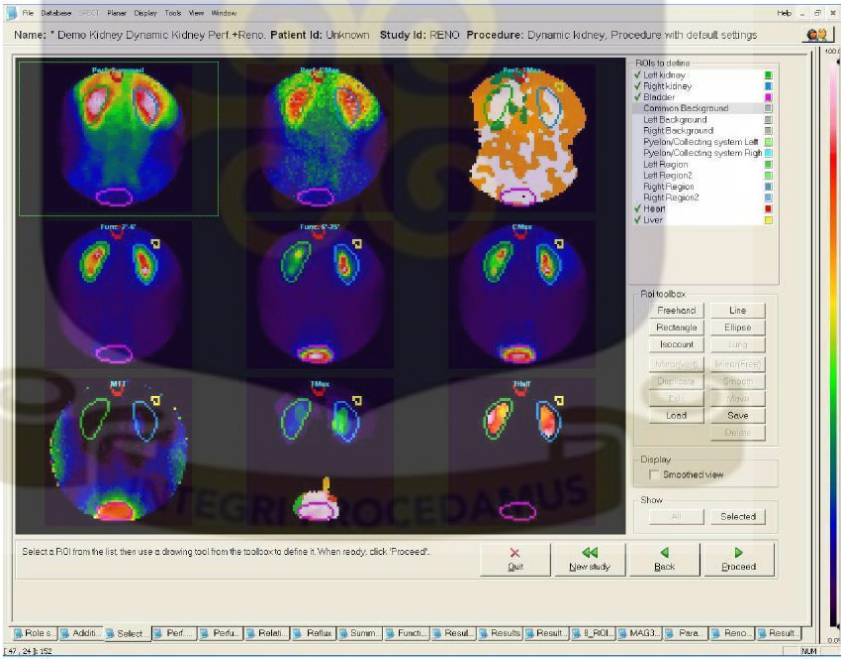

Figure 3.2: ROI selection

Measurement of organs thicknesses with the Hitachi Supra CT

Body and organs thicknesses weremeasured from the CT imageswith Radiant Dicom Viewer software at the Diagnostic RadiologyDepartmentof LamordeHospital in

Niamey as shown in figure 8. Ten (10) patients were scanned and the mean thickness for body and organs were recorded and used for the work.

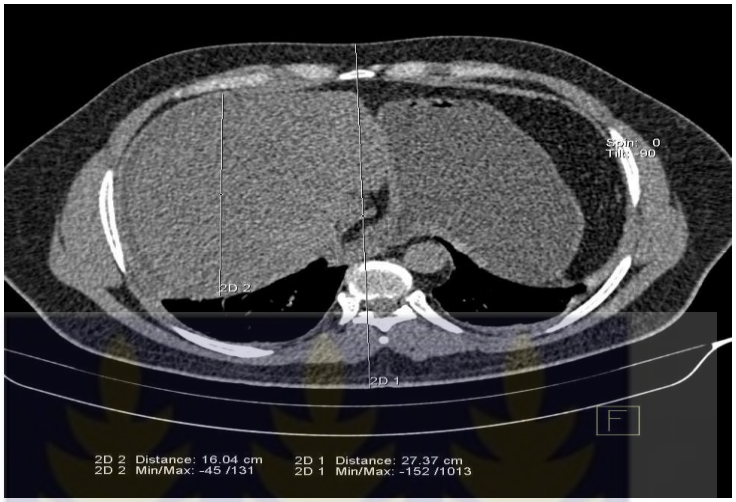

Figure 3.3: Thickness measurement

3.1.3 OLINDA software

Organ Level Internal Dose Assessment Exponential Modeling (OLINDA EXM) is a computer code meant to provide a functionsimilar tothat ofMedical Internal Radiation Dose (MIRDOSE) code. The MIRDOSE performs internal dose calculations according to the MIRD technique for many radionuclides commonly used in nuclear medicine.

The software is used to assess doses to variety of organs such as prostate gland, peritoneal cavity, head/brain, multipart kidney, liver, stomach, pancreas, lung and heart. The software makes use of data from over 200 radionuclides for its dose measurements.

The main use of this program is in the calculation of internal radiation dose estimates for radionuclides used in nuclear medicine. The program has phantom libraries which permit the calculation of these doses for individuals of different age and size and for

women at different stages of pregnancy.Interfaces for OLINDA software are shown in Figure 3.4.

Figure 3.4: OLINDA input form

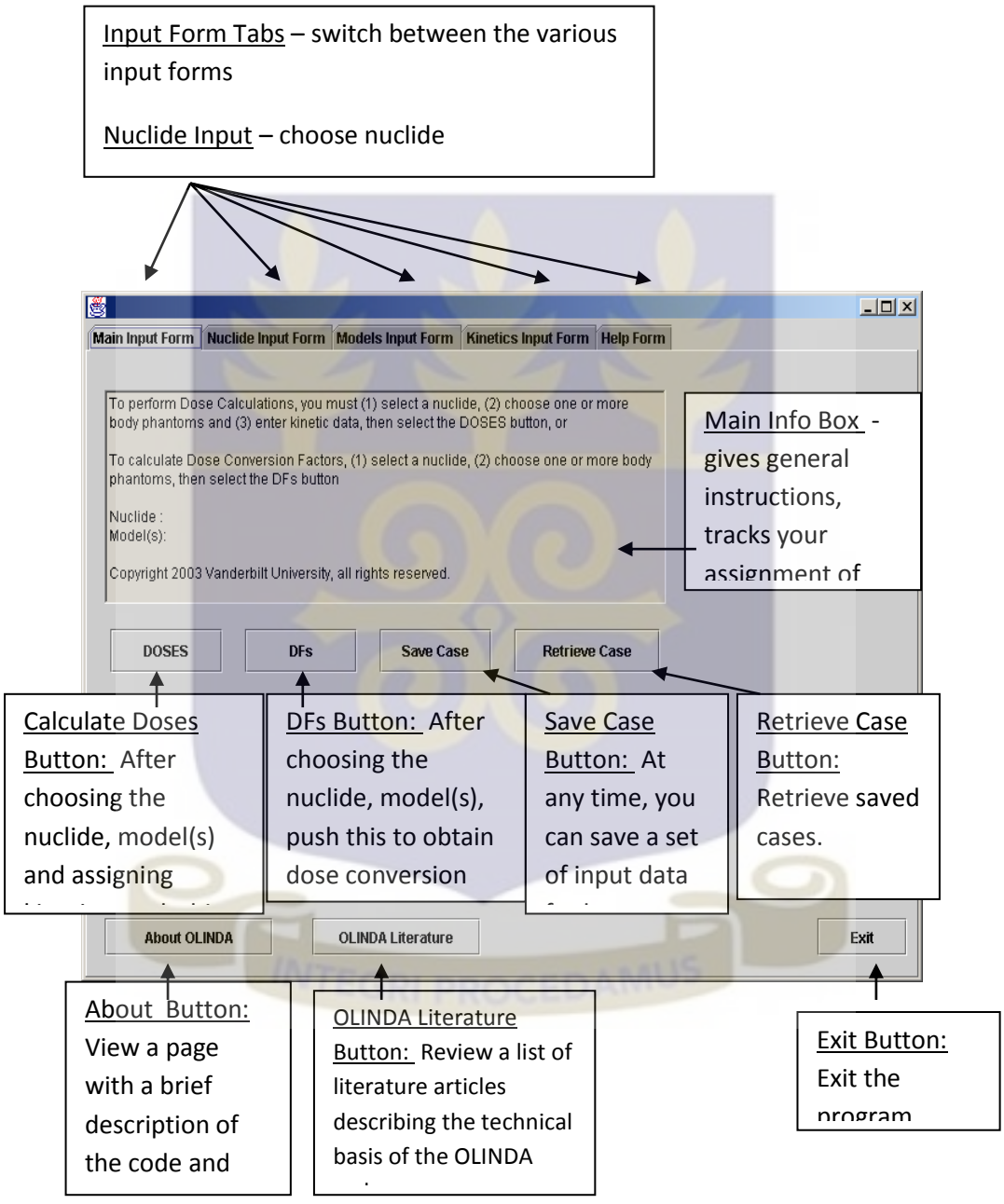

3.2 Methodology

3.2.1 Wholebody scan

The Nuclear Medicine Department of the RadioisotopesInstitute (RII) of Niamey uses Tc-99m Sestamibi to perform Myocardial Perfusion Imaging (MPI). Tc-99m Sestamibi is prepared in the hot laboratory of the departmentaccording to the manufacturer's instructions and administered byintravenous injection to the patient at the maximum predicted heart rate during the stress stage for the procedure. Before performing the imaging, theMediso gamma camera systemequipped with a Low Energy High Resolutioncollimatorsareused to acquire the anterior and posterior planar whole-body images of the patient at ten (10)minutes after administration of the radiopharmaceutical and then two (2) hours and four (4) hours after performing the imaging. For bladder dose assessment, static acquisition is performed after 10 minutes, 20 minutes and 2 hours after the injection.

The Administered activities for patients in this study were 10 mCi for the stressand 30 mCi for the rest examinations.

The Matrix size was256 x 1024 for wholebody scan and 256 x 256 for static acquisition at the speedof 25 cm per minute.

Wholebody scans of patients undergoing SPECT MPI with 10 mCi ^{99m}Tc-Sestamibi during the stress are shown in figure 3.5

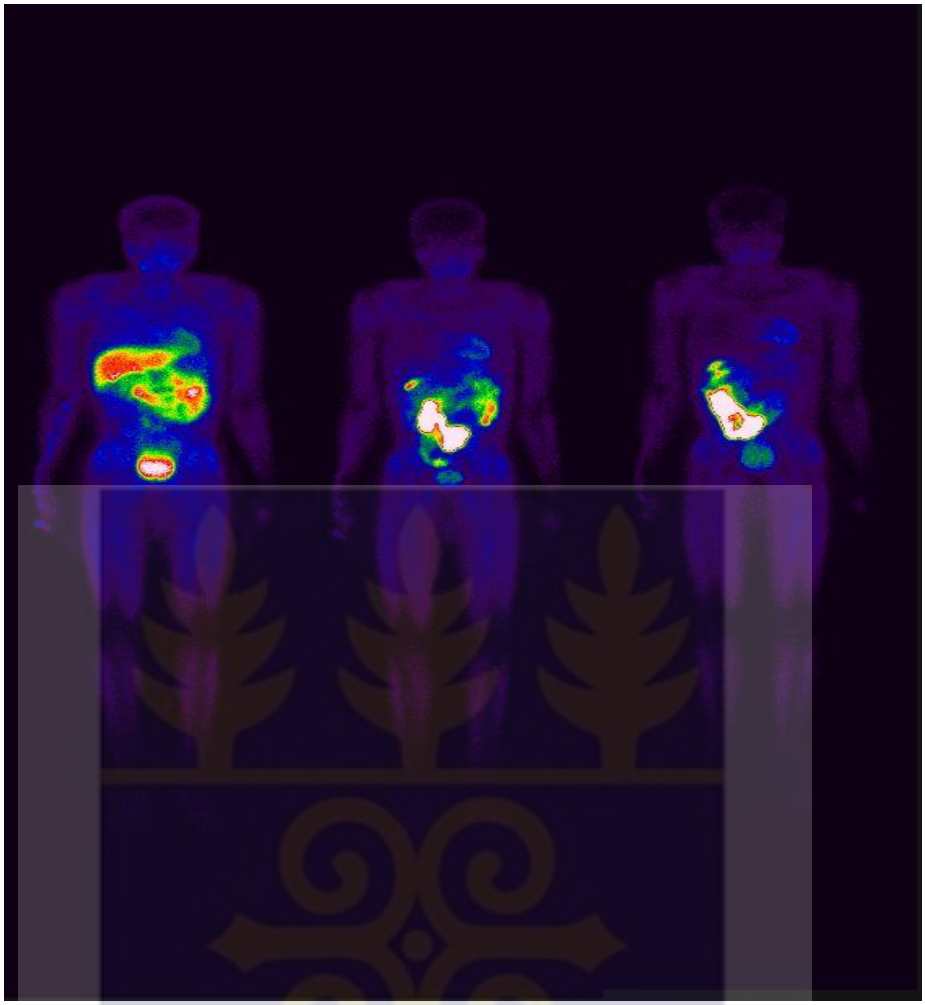

Figure 3.5: Whole-body scanof a patientafter injection of 10 mCi, ^{99m}Tc-Sestamibi 10 min, 2 h and 4 hours (left to right)

3.2.2 Data collection

This study was conducted on 30 adult patients with an average age of 47.6. Whole-body scans of 23 patients wereacquired at 10 minutes, 2 hours and 4 hours on the Mediso Gamma Camera system. The system was again usedto scan 7 patients for bladder static acquisition after 10 minutes, 20 minutes and 2 hours in order to assess the dose to the testes and ovaries.Scans of 10average sized patients were performed for determination of body and organs thicknesses.

Due to ethical reasons, patient names were encoded with ID numbers, with their names hidden. Table 3.1 shows data on the patients sampled for this study.

Table 3.1: Biodata and injected activity of 30 patients

Patient ID	**AGE (years)**	**GENDER**	**Weight** (kg)	**Height (Cm)**	**BMI**
1	45	M	76	168	26.95
2	48	F	77	155	32.08
3	38	M	77	183	22.98
4	55	F	97	173	32.44
5	51	M	77	169	27.01
6	50	M	93	170	32.17
7	57	M	94	174	31.12
8	44	F	86	165	31.61
9	30	F	91	171	31.16
10	53	M	79	184	23.33
11	23	M	55	156	22.60
12	48	M	74	178	23.35
13	38	F	106	166	38.46
14	25	M	98	179	30.58
15	60	M	88	168	31.17

16	43	M	75	175	24.48
17	47	F	57	156	23.42
18	50	F	61	157	24.74
19	60	M	76	184	22.44
20	51	M	78	177	24.84
21	49	F	79	164	29.37
22	32	M	79	168	27.99
23	57	M	81	181	24.72
24	60	F	53	155	22.06
25	60	F	91	175	29.71
26	48	F	83	158	33.24
27	51	F	80	160	31.25
28	52	F	124	170	42.90
29	60	F	58	162	22.10
30	43	F	75	168	22.57
Mean	**47.6**	**15/15**	**80.6±15.8**	**169.5±8.87**	**27.99±5.28**

The average of the patient's weight is 80.6 ±15.8 kg, the average height is 169 ±8.87 cm and the body mass index is 27.99± 5.28. The average age is 47.6 with the maximum age at 60 and the minimum at 23 years in 15 men and 15 women.

3.2.3 Quantitative assessment

Regions of interest were drawn for the heart, liver and bladder on each patient using the ROI statics tools of the Interview®software. Table A1 (in the appendix) shows the selected regions of interest and their respective geometric mean counts (GMCs).

The respective counts of activity for all ROIs were recorded. Geometric mean counts (GMC) of activity for selected ROIs were calculated using anterior and posterior counts. GMC for each selected organ were calculated using Microsoft Excel 2010.

$$\text{GMC} = \sqrt{\text{Anterior Mean Counts} \times \text{Posterior Mean Counts}} \qquad (3.1)$$

Standard Deviation was performed using equation (3.2).

$$SD = \sqrt{\frac{\sum (x - \bar{x})^2}{N}} \qquad (3.2)$$

Where $\bar{x}$ is the mean of N values.

3.2.4 Conversion of counts into activity

In this study, the counts obtained for each patient were converted into activity using conjugate view method. The activities were estimated using equation (3.3).

$$A = \sqrt{\frac{C_A * C_p}{e^{-\mu_e t}}} * \frac{f}{C} \qquad (3.3)$$

In this equation, A is the organs activity in mCi, C_A and C_P are the anterior and posterior view background corrected counts respectively, t is the body anterior–posterior thickness across each organ. Also μ_e is the effective linear attenuation coefficient of Tc-99m in soft tissue, f is equal to $(\mu_e x/2)/\sinh(\mu_e x/2)$ and represents

a correction for the source region attenuation coefficient (μ_e) and source organ thickness (x) and C is the system calibration factor (counts per unit activity).

Determination of body and organ thickness

For body and organ thicknesses were determined in the AP and PA positions, computed tomography scans of 10average sized patients was used. Organs which were considered in this study were heart, liver, kidneys and urinary bladder. The mean body and organ thicknesses were measured and their respective standard deviations were estimated. Table 4 shows the thicknesses of body sections and organs of interest in this study.

Determination of the system calibration factor

A point-source of 5 mCiTc-99m was acquired for a period of 60s with the Mediso gamma camera (Figure 3.6). After the acquisition, the count of the source was recorded and the counts activity found was864kcts. The calibration factor was calculated using equation (3.4).

$$C = \frac{Source\ counts}{known\ Activity} \qquad (3.4)$$

Figure 3.6: Determination of the system calibration factor

3.2.5 Biokinetic model

The biokinetic model (Figure 12) published by *L. Melendez-A. et al* was used to simulate with MATLAB, the transfer of the amounts of ^{99m}Tc-Sestamibi in blood, liver, kidney and bladder.

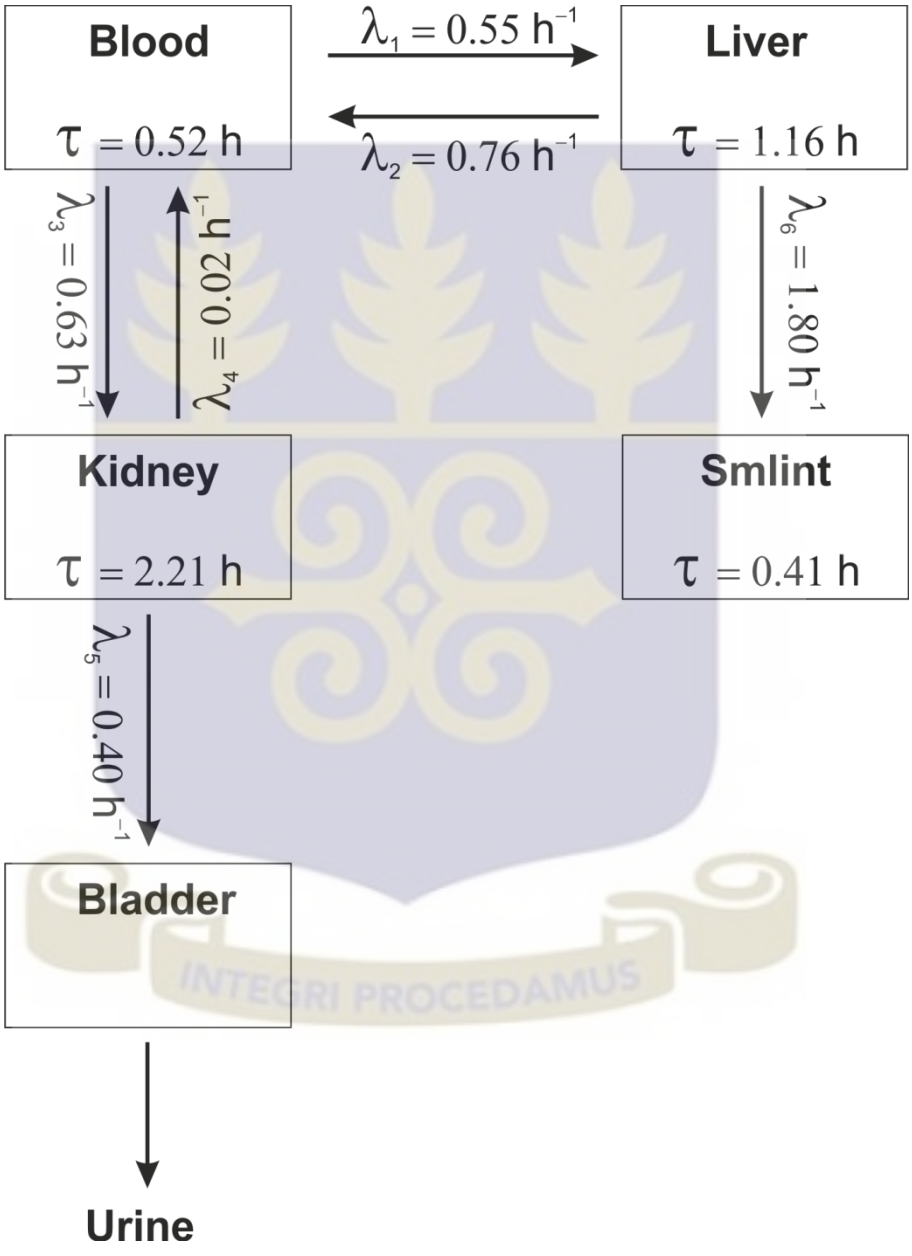

Figure 3.7: Compartmental diagramdescribing the kinetics of ^{99m}Tc-Sestamibi through the body.

The simulation of the amounts of Tc-99m activity in Blood (Bd), liver (Li), Kidney (Ki) and Urinary Bladder (Ub) was done by these equations:

$$\frac{d_{q_{Bd}}}{dt} = -(\lambda_R + \lambda_1 + \lambda_3)q_{Bd} + \lambda_2 + \lambda_4 \quad (3.6)$$

$$\frac{d_{q_{Li}}}{dt} = -(\lambda_R + \lambda_6 + \lambda_2)q_{Li} + \lambda_1 \quad (3.7)$$

$$\frac{d_{q_{Kid}}}{dt} = -(\lambda_R + \lambda_4 + \lambda_5)q_{Kid} + \lambda_3 \quad (3.8)$$

$$\frac{d_{q_{UB}}}{dt} = -\lambda_R + \lambda_5 \quad (3.9)$$

Equations 3.6, 3.7, 3.8 and 3.9 can be reorganized again as below and solved by the MATLAB program.

$$\begin{pmatrix} dq_{Bd}/dt \\ dq_{Li}/dt \\ dq_{Kd}/dt \\ dq_{Bl}/dt \end{pmatrix} = \begin{pmatrix} -\lambda 1 - \lambda 3 - \lambda R & \lambda 2 & \lambda 4 & 0 \\ \lambda 1 & -\lambda 2 - \lambda R & 0 & 0 \\ \lambda 3 & 0 & -\lambda 4 - \lambda 5 - \lambda R & 0 \\ 0 & 0 & \lambda 5 & -\lambda R \end{pmatrix} \begin{pmatrix} q_{Bd} \\ q_{Li} \\ q_{Kd} \\ q_{Bl} \end{pmatrix}$$

λ_1,λ_2 ,λ_3, λ_4, λ_5, $\lambda_6$are the transfer rate constants and λ_R is the physical decay constant of the Tc-99m radionuclide published by *L. Melendez-A et. al*

3.2.6 Determination of the residence time

Determination of the residence time of Sestamibi in the heart, liver and kidneys was estimated on 23 adult patients (8 females and 15 males) with an average age of **45.8** years.

The residence time of Sestamibi in the bladder was estimated on 7 patients (6 females and 1 male) with the average age of **53.4** years in order to assess the dose to the testes and ovaries. All the patients recruited for this study were referred from others hospitals to undergo myocardial perfusion imaging. All patients signed a consent form after receiving information about the aim of the study. The injected radionuclide activity for the stress was 10 mCi of ^{99m}Tc-Sestamibi and for the rest study was 30 mCi. Patients were imaged with a dual-heads gamma camera (Mediso), equipped with low-energy high resolution collimators. A 15% energy window centered over the 140 keVphotopeak of ^{99m}Tc was used.

Patients were scannedat three different time point for heart, liver and kidney dose assessments. Patients were scanned at 10 minutes, 2 hour and 4 hours after radionuclide injection for bladder dose assessment, patients were scanned 10 minutes, 20 minutes and 2 hours after injection of radionuclide.

The determination of the radionuclide activity in organs involved, regions of interest were drawn on images obtained at three time point. The ROIs were drawn around source-organs such as heart, liver, kidneys and bladder.

The uptake activity at different time points were estimated for the heart, liver, kidneys and bladder and used to generate the time-activity curves. The time-activity curves were fitted by Microsoft Excel (2010 version) and used to estimate cumulative activity in each organ of interest. Functional fitting procedure was used to generate

expressions for calculating the cumulated activity value for heart, liver, bladder and kidney and for each patient.

Residence time for radionuclide in the organs were estimatedwith equation 3.10.

$$\tau = \frac{\tilde{A}}{A_0} \tag{3.10}$$

Where τ: residence time, Ã: cumulated activity and A_0: injected activity

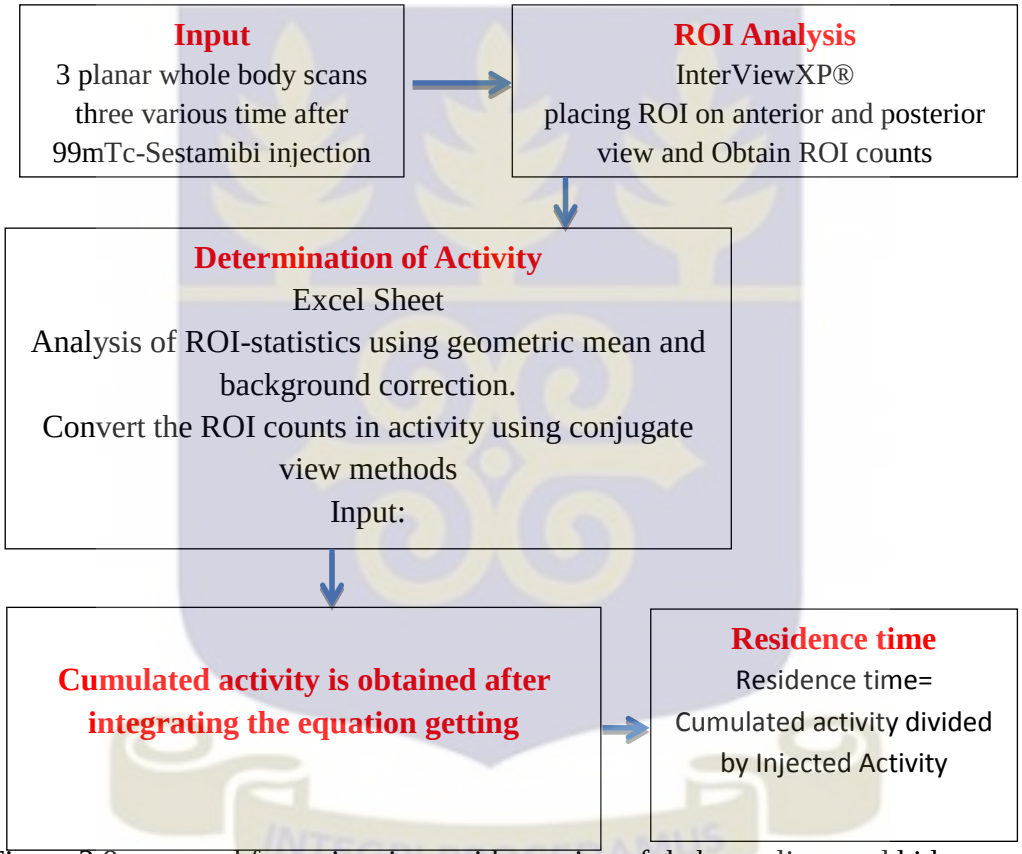

Figure 3.8: protocol for estimating residence timeof theheart, liver and kidneys

3.2.7 Dose calculation

Dose calculation was performed by assuming that the average mass of the patient is 70kg. Standard value (S-V) for the heart, liver, kidney and bladderwhichwere used to estimate the dose receiving by the source-organs using the OLINDA software.

Table 3.2: Estimated radiation dose to certain organs according to Mirdose3 using ^{99m}Tc-Sestamibi

Target organs	Estimated radiation dose
Thyroid	2.22E-03
Bladder wall	5.37E-03
Kidneys	23.1E-03
Liver	8.19E-03
Heart wall	4.95E-03
Lungs	2.75E-03
ovaries	62.4E-03
Spleen	8.62E-03
Testes	7.90E-03

According to the MIRDOSE 3 software, the radiation dose to different organsis below using equation 3.10

$$\overline{D}_h = \sum_k \tilde{A}_k * S(h \leftarrow k) \qquad (3.10)$$

For Tc-99m Sestamibiwholebody scan, the source organs well observed are: Bladder, heart, kidneys, liverand the intestine.

3.2.8 Determination of the Uncertainty of Biokinetic models for ^{99m}Tc-Sestamibi

Mathematical and Biokinetic or compartmental models are developed by the ICRP and MIRD committee. These models are used to calculate the residence time or cumulated activity in the source organ per unit administered activity (Stabin, 2008).

A series of physical factors contribute to the difference between measured activity and actual activity in source regions based on planar scintigraphy. Accurate estimation of the activity in an organ from the measured counting rate requires correction for the system calibration factor, attenuation, scatter, background activity, organ and patient thickness and physical decay of the radionuclide used (Buijs et al, 1998).

The uncertainties of the parameters which contribute to the absorbed dose uncertainty can be allocated to two main parts:

1- The uptake, distribution and retention of the radiopharmaceuticals in organs and tissues;
2- The mass and position of the organs and tissues.

The total uncertainty in individual dose estimated can be reduced to a value of perhaps ± 10-20% (Stabin, 2008).

For this study, uncertainties of background correction and attenuation correction and scatter correction are estimated.

CHAPTER FOUR: RESULTS AND DISCUSSION

4.1 Introduction

This chapter presents the results of the estimated ^{99m}Tc-Sestamibi activities in the source-organs (heart, liver, kidney and bladder) and the absorbed dose per unit administered activity estimated for the critical organsusing MIRD formalism and OLINDA software analysis. The results have been discussed in detail and the relationship between the experimental and theoretical activity estimates in the heart, liver, kidney and bladder have been estimated.

4.2 Results

4.2.1 Body and organs thickness

Thicknesses of the patient bodyweremeasured from scansof10 patients from the Department of Diagnostic Radiology of Lamorde National hospital.Computed tomography images of the thorax were used to determine thickness of the heart, abdominal CT images for the thickness of kidney, and pelvic CT images for the thickness of bladder. The average estimated value of the body and organs thicknesses arepresented in Table 4.1. Detailed estimates of the individual thicknesses of each patient are shown in appendix 1

Table 4.1: Average thickness for the body and organs thickness for 10 sized patient CT scan

	Region of interest			
Body section	Abdomen	Pelvis	Thorax	
Average thickness(cm)	21±0.21	23±1.48	21.9±0.57	
Organ	Kidney	Bladder	Heart	Liver
Average thickness(cm)	5.5±1.06	8.5±1.13	9.7±1.57	15.7±1.41

From Table 4.1, body thickness from CT scans of the 10 patients for the abdomen, pelvic and thorax were 21 cm±0.21, 23 cm±1.48 and 21.9±0.57 cm respectively. The corresponding thickness for the kidney, bladder, heart and liver were 5.5±1.06 cm, 8.5±1.13 cm, 9.7 ±1.57 cm and 15.7±1.41 cm respectively. These values are consistent with Larsson et al, *2012*who measured a kidney thicknesses average of 5.54 cm in a study involving the measurement of kidney of 33 patients.The measured Values are also consistent with the study ofRonald et al, 1995.

The values of these thicknesses were used to estimate the attenuation coefficient of Tc-99m where the conjugate view approach was applied in converting counts into radionuclide activity for the heart, liver, kidney and bladder ROIs.

4.2.2 Activity of the source- organs

InterViewXP® ROIs tools was used to get the counts statistics after scanning patients and drawing the ROIs around the source organs (heart, liver, kidneys and bladder).

The conjugate view method was used to convert the counts (cts) into activity (µCi) as shown in tables from 4.2 to 4.9. Table A1 in the appendix 2 details the counts (cts) of

the ROIs in the different source organs (heart, liver, kidneys and bladder) for each patient.

Table 4.2: Estimated radionuclide activities in organs for patients, ten minutes post-injection of 10 mCi Tc-99m Sestamibi

ID	SEX	AGE	ACTIVITY in μCi		
			Heart	Liver	Kidneys
1	M	45	208.57	630.3	401.25
2	F	48	250.21	668.49	398.89
3	M	38	174.50	628.09	519.53
4	F	55	166.55	642.90	550.22
5	M	51	224.66	629.96	480.29
6	M	50	205.08	496.01	487.73
7	M	57	162.74	623.26	559.26
8	F	44	241.23	816.51	567.51
9	F	30	243.81	868.34	498.16
10	M	53	137.19	950.71	465.86
11	M	23	242.02	562.80	497.96
12	M	48	240.60	740.74	573.45
13	F	38	273.52	661.89	512.09
14	M	25	183.95	526.59	468.61
15	M	60	266.20	953.68	596.04
16	M	43	249.06	777.65	445.26
17	F	47	161.61	411.13	509.24
18	F	50	77.35	635.45	575.15
19	M	60	158.40	436.20	457.36
20	M	51	304.35	640.40	477.88
21	F	49	190.14	447.21	486.23
22	M	32	243.57	643.02	483.73
23	M	57	398.60	634.58	491.43
Average		45.8	**217.56±134.37**	**653.30±3.03**	**500.14±63.76**

Table 4.2 shows the estimated activities (µCi)in the heart, liver, kidneys, ten minutes after injection of 10 mCi of ^{99m}Tc-Sestamibi during SPECT MPI. These uptakes radionuclide activities uptake represent 2.17% for the heart, 6.53% for the liver and 5% for the kidneys of the injected activities. Wackers et al.,1989 , found respectively 1.5±0.4%, 5.9±2.9% and 10.6±2.2% for the heart, liver and kidneys five minutes after injection of Sestamibi.

Table 4.3: Estimated bladder activity after injection of 10 mCi Tc-99m Sestamibi

ID	SEX	AGE	ACTIVITY in µCi		
			10 minutes	20 minutes	120 minutes
24	F	60	899.46	1385.31	1725.51
25	F	60	981.33	1184.98	1964.32
26	F	48	656.63	805.51	1050.72
27	F	51	813.77	882.70	1059.10
28	F	52	279.44	680.25	1117.39
29	M	60	135.54	859.87	1054.32
30	M	43	383.11	900.36	1234.81
Average		53	592.75±365.11	957±342.91	1315.17±346.97

Table 4.3 shows the estimated radionuclides activitiesin the bladder, 10minutes, 20 minutes and 120 minutes after injection of 10 mCi of ^{99m}Tc-Sestamibi during SPECT MPI. The urinary bladder uptake at 10 minutes, 20 minutes and 120 minutes represents 5.92%, 9.57% and 13.15% respectively of the injected activity

Table 4.4: Estimated organs activities for patients, 120 minutes post injection of 10 mCi Tc-99m Sestamibi

ID	SEX	AGE	ACTIVITY in µCi		
			Heart	Liver	Kidneys
1	M	45	151.20	451.06	171.90
2	F	48	210.14	480.65	213.01
3	M	38	110.46	399.41	236.01
4	F	55	92.12	381.80	230.30
5	M	51	90.77	458.24	225.28
6	M	50	152.20	362.55	205.78
7	M	57	112.86	496.54	262.69
8	F	44	163.76	567.25	269.06
9	F	30	183.07	562.66	229.67
10	M	53	42.91	266.73	217.61
11	M	23	176.85	369.21	220.54
12	M	48	190.55	421.11	269.77
13	F	38	186.95	364.79	217.54
14	M	25	146.05	349.98	212.43
15	M	60	215.29	563.50	264.59
16	M	43	170.40	553.72	164.06
17	F	47	88.02	342.34	235.31
18	F	50	35.78	385.59	264.32
19	M	60	84.38	324.99	203.72
20	M	51	210.65	474.25	207.87
21	F	49	153.89	273.95	200.32
22	M	32	170.10	421.87	202.82
23	M	57	278.44	372.07	219.88
Average		45.8	**148.56±89.97**	**419.32±55.85**	**223.67±33.93**

Table 4.4 shows the estimated activities(µCi) in the heart, liver, kidneys at120 minutes after injection of 10 mCi of ^{99m}Tc-Sestamibi during SPECT MPI and represented an uptake of 1.48%, 4.19% and 2.23% of the injected activity.

Table 4.5: Estimated organs activities for the patients 240 minutes post-injection of 10 mCi Tc-99m Sestamibi

ID	SEX	AGE	ACTIVITY in µCi		
			Heart	Liver	Kidneys
1	M	45	126.80	358.07	41.55
2	F	48	41.65	127.86	52.50
3	M	38	59.75	306.12	65.80
4	F	55	37.82	281.51	74.84
5	M	51	29.17	340.62	55.97
6	M	50	121.71	151.53	61.38
7	M	57	54.14	118.13	63.05
8	F	44	27.87	149.05	81.51
9	F	30	29.95	158.24	71.70
10	M	53	27.65	58.68	55.52
11	M	23	99.16	249.52	62.14
12	M	48	101.19	219.64	82.81
13	F	38	116.48	246.40	69.89
14	M	25	103.53	69.80	71.57
15	M	60	29.39	194.20	74.13
16	M	43	23.77	175.13	52.75
17	F	47	53.12	187.96	66.97
18	F	50	14.49	258.65	89.93
19	M	60	43.16	226.29	50.62
20	M	51	188.64	347.10	58.68
21	F	49	99.55	137.96	55.78
22	M	32	70.11	166.63	54.08
23	M	57	183.34	209.32	51.73
Average		45.8	**73.15±38.98**	**206.02±105.18**	**63.69±7.20**

Table 4.5 shows the estimated activities(µCi) in the heart, liver, Kidneys, 240 minutes after injection of 10 mCi of ^{99m}Tc-Sestamibi during SPECT MPI. The uptake in the

organs represents 0.73% for the heart, 2.06% for the liver and 0.63% for the kidneys of the injected activity.

Table 4.6: Estimated organs activities for the patients 10 minutes post injection of 30 mCi Tc-99m Sestamibi

ID	SEX	AGE	ACTIVITY in µCi		
			Heart	Liver	Kidneys
1	M	45	1328.04	3971.63	1284.01
2	F	48	885.55	6580.55	1077.00
3	M	38	878.89	4411.13	1423.52
4	F	55	1261.51	4740.51	1540.62
5	M	51	1347.31	4264.92	1291.98
6	M	50	1419.93	4787.71	1472.95
7	M	57	598.69	3790.10	1683.38
8	F	44	492.93	3571.15	1719.55
9	F	30	786.02	3629.99	1444.67
10	M	53	570.42	7920.02	1425.54
11	M	23	929.34	4239.78	1020.81
12	M	48	1423.10	5708.14	1766.23
13	F	38	1461.51	4810.32	1469.70
14	M	25	994.61	3764.52	1091.86
15	M	60	1470.36	6192.62	1841.77
16	M	43	1031.99	4450.33	1090.90
17	F	47	842.80	4216.17	1522.62
18	F	50	476.18	4953.95	1731.21
19	M	60	693.34	3634.60	1376.64
20	M	51	1123.44	4123.73	1462.30
21	F	49	1113.59	4447.03	1458.69
22	M	32	1717.79	3872.15	1407.66
23	M	57	968.76	3151.02	1145.03
Average		45.8	**1035.48±254.05**	**4575.31±580.26**	**1423.85±98.27**

Table 4.6 shows the estimated activities (µCi)in the heart, liver, Kidneys, 10 minutes after injection of 30 mCi of ^{99m}Tc-Sestamibi during SPECT MPI. The organs uptake

is 3.45% for the heart, 15.25% for the liver and 4.74% for kidneys of the injected activity.

Table 4.7: Estimated bladder activity after injection of 30 mCi Tc-99m Sestamibi

ID	SEX	AGE	ACTIVITY in µCi		
			10 minutes	20 minutes	120 minutes
24	F	60	2698.38	3463.4	5003.97
25	F	60	2306.12	3673.43	3928.60
26	F	48	1838.56	2497.08	2942.01
27	F	51	2481.99	3089.45	3060.79
28	F	52	810.37	1891.09	3374.51
29	M	60	414.75	2545.21	3236.76
30	M	43	1225.95	2602.04	3704.43
Average		53	1682.30±1041.17	2823.08±609.07	3607.30±918.91

Table 4.7 shows the estimated activities (µCi)in the bladder, 10minutes, 20 minutes et 120 minutes after injection of 30 mCi of ^{99m}Tc-Sestamibi during SPECT MPI. The urinary bladder uptake is 5.60% 10 minutes after 30 mCi injection, 9.41% 20 minutes after injection and 12.02% after 120 minutes of the injected activity.

Table 4.8: Estimated organs activities for patients 120 minutes post-injection of 30 mCi Tc-99m Sestamibi

ID	SEX	AGE	ACTIVITY in µCi		
			Heart	Liver	Kidneys
1	M	45	626.62	1383.62	543.8
2	F	48	374.59	1391.35	517.73
3	M	38	114.73	1594.79	497.57
4	F	55	497.13	601.68	575.75
5	M	51	595.38	1934.78	673.58
6	M	50	642.14	807.92	617.33
7	M	57	390.93	818.82	630.28
8	F	44	174.66	1917.17	777.57
9	F	30	412.63	1255.64	675.22
10	M	53	300.31	781.25	613.65
11	M	23	415.71	1485.18	513.85
12	M	48	477.40	1374.76	714.89
13	F	38	109.36	1423.75	665.68
14	M	25	349.61	1001.99	635.16
15	M	60	296.79	1371.73	769.96
16	M	43	249.16	1444.71	388.83
17	F	47	291.43	996.62	696.51
18	F	50	118.16	481.67	711.02
19	M	60	545.81	454.49	478.74
20	M	51	727.38	700.39	642.31
21	F	49	217.81	613.30	418.67
22	M	32	304.15	442.71	612.52
23	M	57	553.99	1365.80	633.24
Average		45.8	**381.99±51.36**	**1114.96±12.60**	**608.86±63.24**

Table 4.8 shows the estimated activities(µCi) in the heart, liver, kidneys, 120 minutes after injection of 30 mCi of ^{99m}Tc-Sestamibi during SPECT MPI. The average uptake

for the heart represents 1.27%, 3.71% for the liver and 2.02% for the kidneys of the injected activity.

Table 4.9: Estimated organs activities for the patients 240 minutes post-injection of 30 mCi Tc-99m Sestamibi

ID	SEX	AGE	ACTIVITY in µCi		
			Heart	Liver	Kidneys
1	M	45	158.48	391.88	116.34
2	F	48	115.82	320.30	135.98
3	M	38	77.48	293.70	200.68
4	F	55	153.84	278.89	176.63
5	M	51	177.28	244.31	106.34
6	M	50	449.90	190.11	157.13
7	M	57	126.84	248.84	167.1
8	F	44	167.72	190.81	161.39
9	F	30	172.14	185.06	213.67
10	M	53	126.51	231.99	160.45
11	M	23	51.93	355.70	189.54
12	M	48	55.30	243.41	240.99
13	F	38	50.92	250.30	213.18
14	M	25	60.48	296.76	216.13
15	M	60	83.11	250.01	229.08
16	M	43	103.31	276.87	138.73
17	F	47	101.92	300.55	206.94
18	F	50	139.33	231.16	268.89
19	M	60	57.88	270.84	152.89
20	M	51	192.77	263.05	140.25
21	F	49	66.98	249.85	171.82
22	M	32	147.88	217.19	161.17
23	M	57	80.42	288.19	108.12
Average		45.8	**126.88±55.19**	**263.90±73.31**	**175.37±5.81**

Table 4.9 shows the estimated activities(µCi) in the heart, liver, Kidneys, 240 minutes after injection of 30 mCi of ^{99m}Tc-Sestamibi during SPECT MPI. The heart uptake

represents 0.42%, 0.87% for the liver and 0.58% for the kidneys of the injected activity.

These uptakes are observed to be closer to whatWackers et al., 1989, found 5 minutes and 240minutes after injection of 10 mCi and 30 mCi of ^{99m}Tc-sestamibi.

The activity in the liver is higher than the reminder source-organs because majority (50-65 %) of the ^{99m}Tc-Sestamibi injected is eliminated through the extravascular system (liver and digestive system), than the activity of bladder, kidneys and heart respectively, Bucerius et al, 2012.

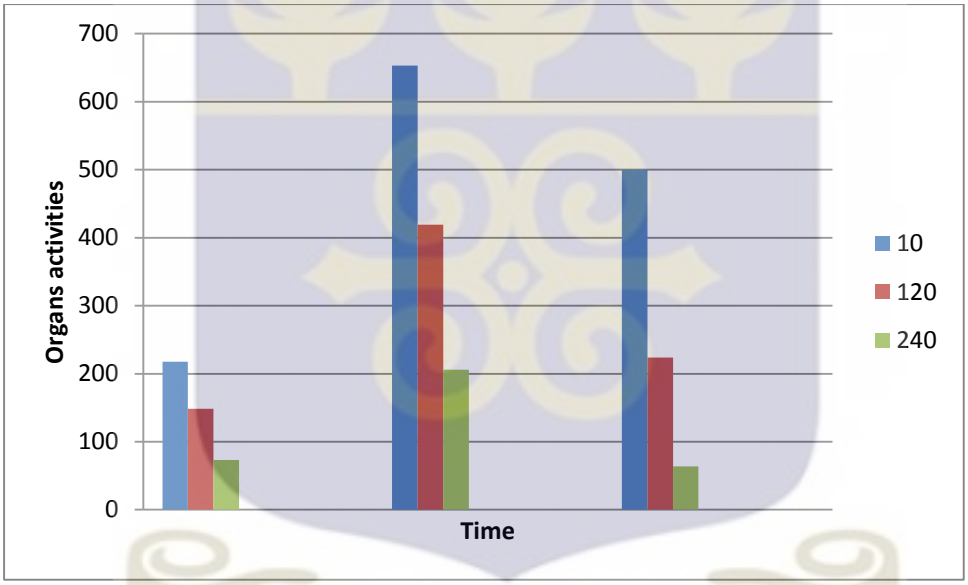

Figure 4.1: Radionuclide activities in the heart, liver and kidneys during myocardial perfusion imaging with ^{99m}Tc-Sestamibi.

Figure 4.1 shows the mean activity in the heart, liver and kidneys after injection of 10 mCi of ^{99m}Tc-Sestamibi at the different time points(10 minutes, 120 minutes and 240 minutes). This figure shows that liver received the highest activity and the least is theheart.

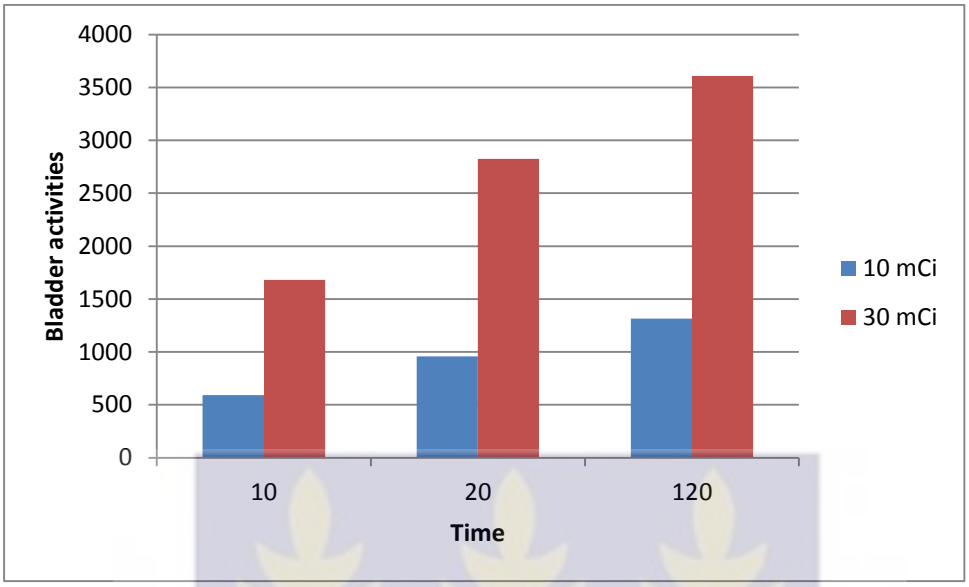

Figure 4.2: Activity in the bladder during myocardial perfusion imaging with ^{99m}Tc-Sestamibi.

Figure 4.2 shows the activity in the bladder 10 minutes, 20 minutes and 120 minutes after injection of 10 mCi and 30 mCi. The bladder is a temporary reservoir, so the activity is accumulated until the patient urinated.

4.2.3 Cumulative activity estimation

The radiation dose delivered to a target organ depends on the amount of activity present in the source organ and on the length of time for which the activity is present. The product of these two factors is the cumulative activity in the source organ.

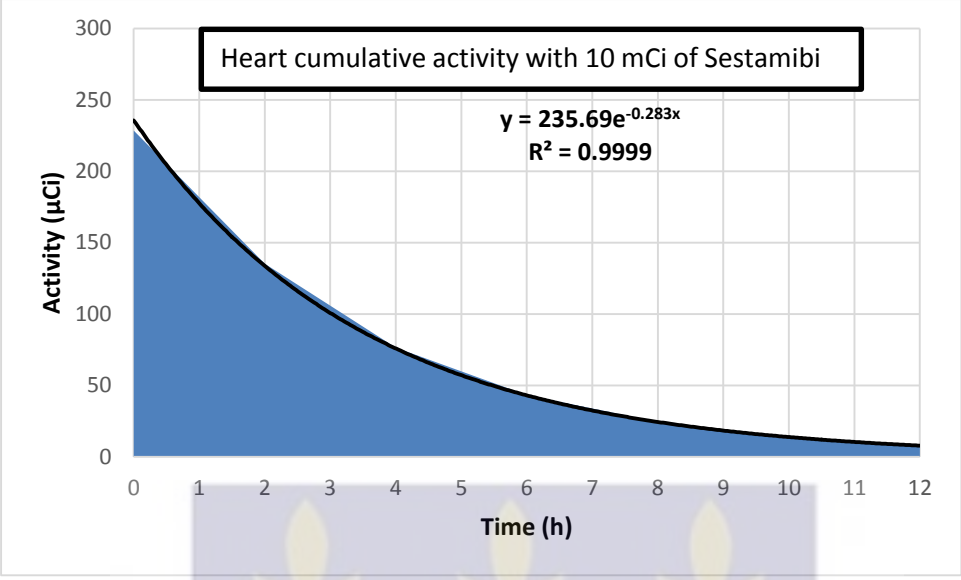

Figure 4.3.Cumulative activity estimation in the heart after injection of 10 mCi of ^{99m}Tc-Sestamibi

After fitting the time activity curve, the equation is then recorded:

$y = 235.69e^{-0.283x}$(4.1);

The integration from 0-∞ of equation 1 gives: 832.82 µCi/h

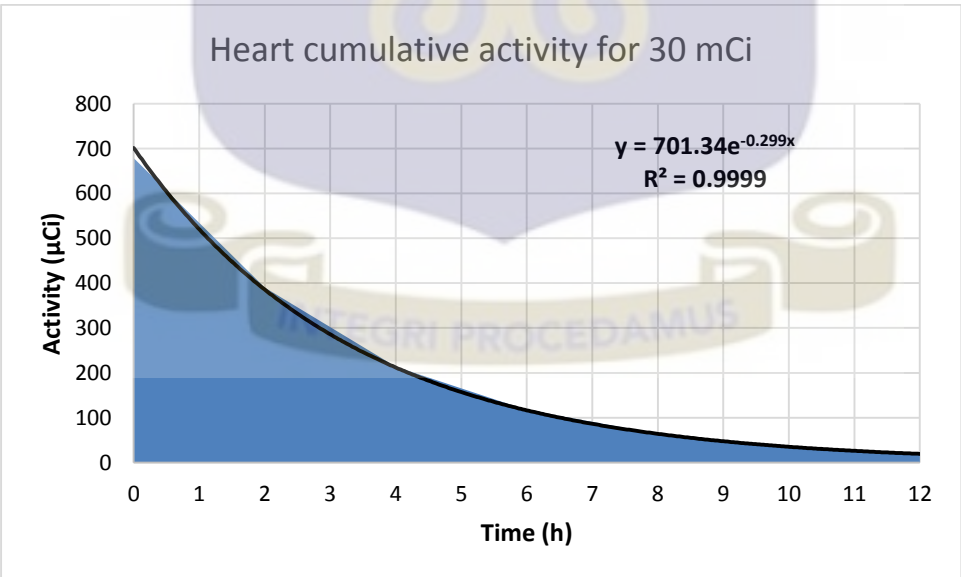

Figure 4.4. Heart cumulative activity estimation after injection of 30 mCi of ^{99m}Tc-Sestamibi

After fitting the time activity cure, the equation is then recorded:

$y = 701.34e^{-0.299x}$(4.2);

The integration from 0-∞ of equation 2 gives: 2345.61 µCi/h.

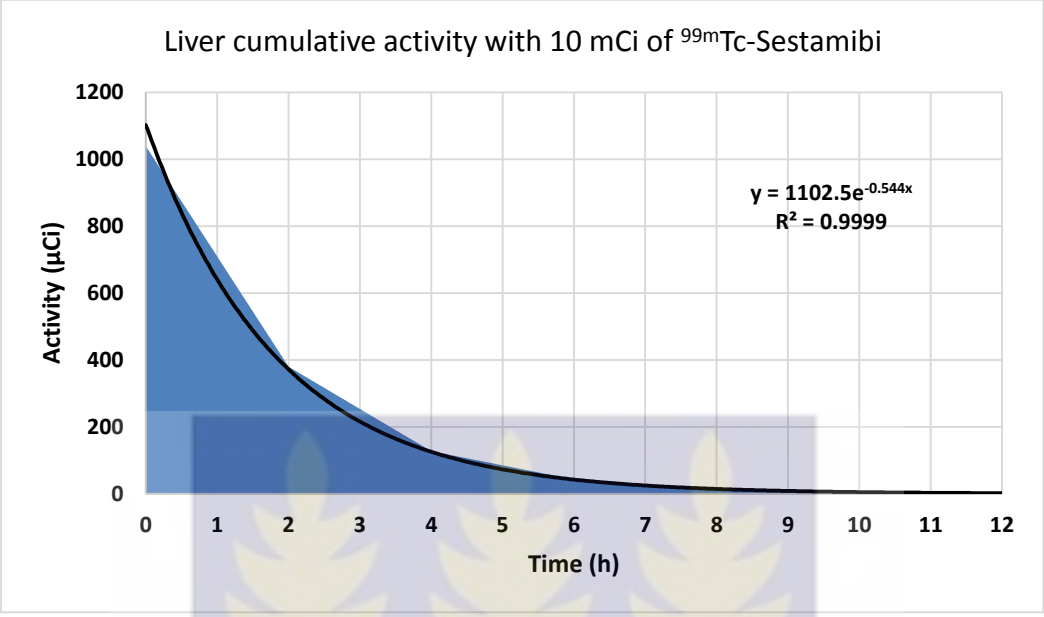

Figure4.5 Liver cumulative activity estimation after injection for 10 mCi of ^{99m}Tc-Sestamibi

After fitting the time activity cure, the equation is then recorded:

$y = 1102.5e^{-0.544x}$(4.3);

The integration from 0-∞ of equation 3 gives: 2026.65 µCi/h

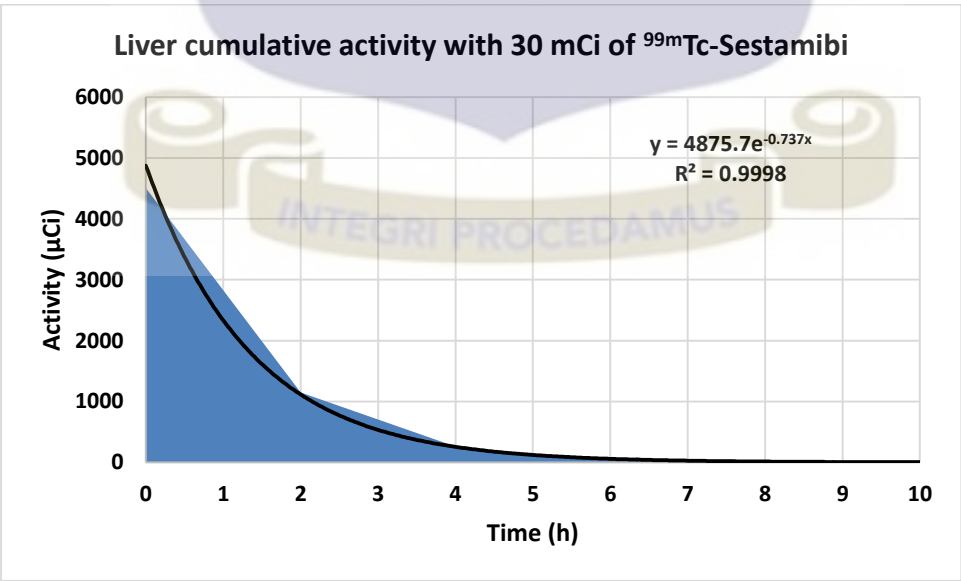

Figure4.6 Liver cumulative activity estimation after injection of 30 mCi of ^{99m}Tc-Sestamibi

After fitting the time activity cure, the equation is then recorded:

$y = 4875.7e^{-0.737x}$(4.4);

The integration from 0-∞ of equation 4 gives: 6615.60µCi/h

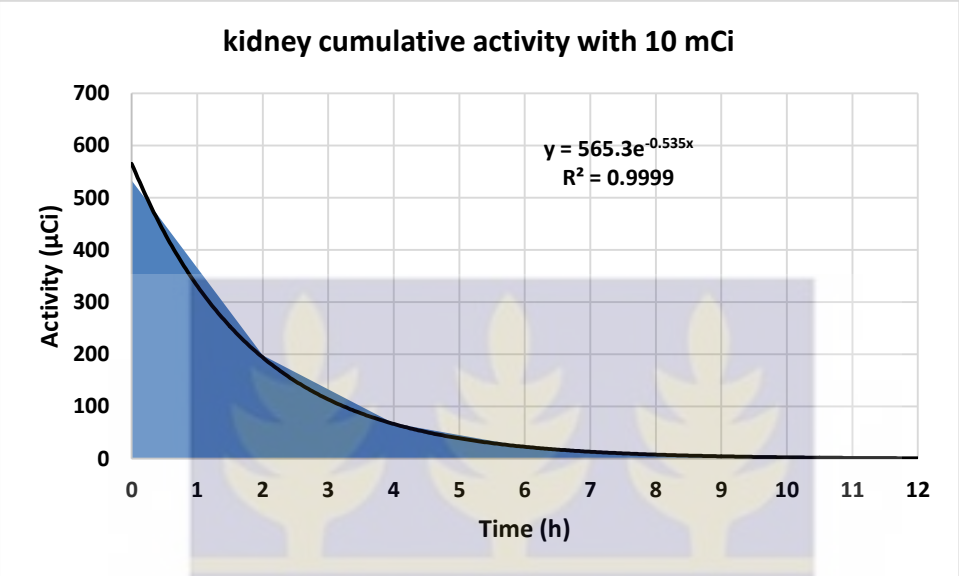

Figure4.7 Kidneys cumulative activity estimation after injection of 10 mCi of ^{99m}Tc-Sestamibi

After fitting the time activity cure, the equation is then recorded:

$y = 565.3e^{-0.535x}$(4.5);

The integration from 0-∞ of equation 5 gives: 1056.63 µCi/h.

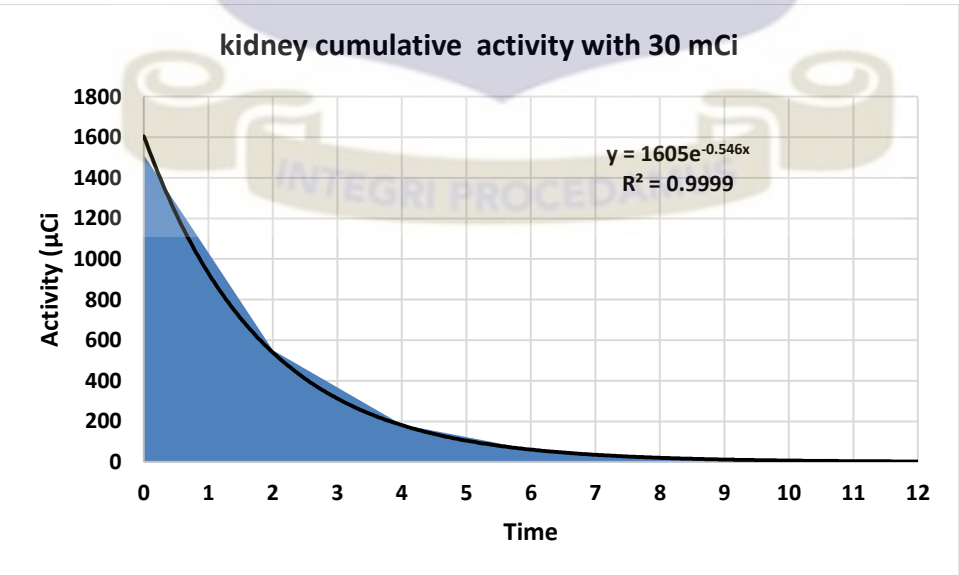

Figure4.8 Kidneys cumulative activity estimation after injection of 30 mCi of ^{99m}Tc-Sestamibi

After fitting the time activity cure, the equation is then recorded:

$y = 1605e^{-0.546x}$(4.6);

The integration from 0-∞ of equation 6 gives: 2939.56µCi/h.

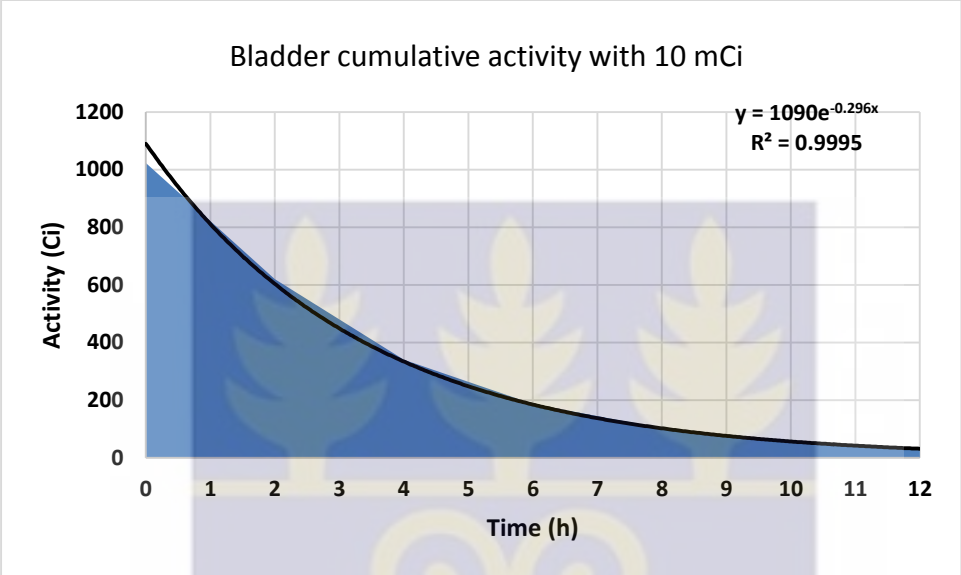

Figure4.9 Bladder cumulative activity estimation after injection of 10 mCi of ^{99m}Tc-Sestamibi

After fitting the time activity cure, the equation is then recorded:

$y = 1090e^{-0.296x}$(4.7);

The integration from 0-∞ of equation 7 gives: 3682.43 µCi/h

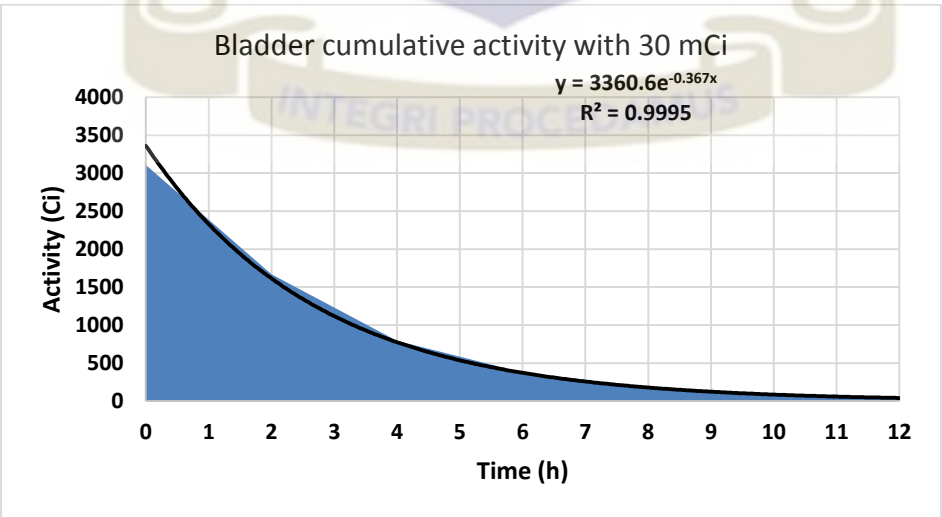

Figure4.10 Bladder cumulative activity estimation after injection of 30 mCi of ^{99m}Tc-Sestamibi

After fitting the time activity cure, the equation is then recorded:

$y = 3360.6e^{-0.367x}$(4.8);

The integration from 0-∞ of equation 8 gives: 9156.94µCi/h

4.2.4 Residence time of ^{99m}Tc-Sestamibi in the heart, liver, kidneys and bladder during myocardial perfusion imaging (MPI)

The residence time (τ) is equal to $\tilde{A}/A_0$(4.9)

Table 4.10: Calculation of residence time of the heart, liver, kidneys and bladder

Source-organs	Cumulative ctivity(µCi/h)		Residence time (τ)	
	For 10 mCi	For 30 mCi	For 10 mCi	For 30 mCi
Heart	832.82	2345.61	0.0832	0.0782
Liver	2026.65	6615.60	0.2027	0.2205
Kidneys	1056.63	2939.56	0.1056	0.0979
Urinary Bladder	3682.43	9156.94	0.3682	0.3052

Table 13 shows that the residence time did not change with the quantity of activity but with the tracer.

The residence time for the kidney and bladder were estimated in order to assess the radiation dose of target- organs. The average residence times estimated for the heart, liver, kidneys and bladder were 0.0807 hour, 0.2116 hour, and 0.1017 hour and0.3367 hour respectively.

These residence times are close to which Ronald et Al, *1995*, found and were 0.086 hour for heart, 0.222 for kidney, 0.304 for liver and 0.343 for urinary bladder.

4.2.5 ^{99m}Tc-Sestamibi Biokinetic model

Time-activity curve for the study was obtained from MATLAB simulation of the biokinetic model published bySydoff, 2013 andRohe et al, *1995*. The MATLAB code of time-activity stimulation curve is found in Appendix 3

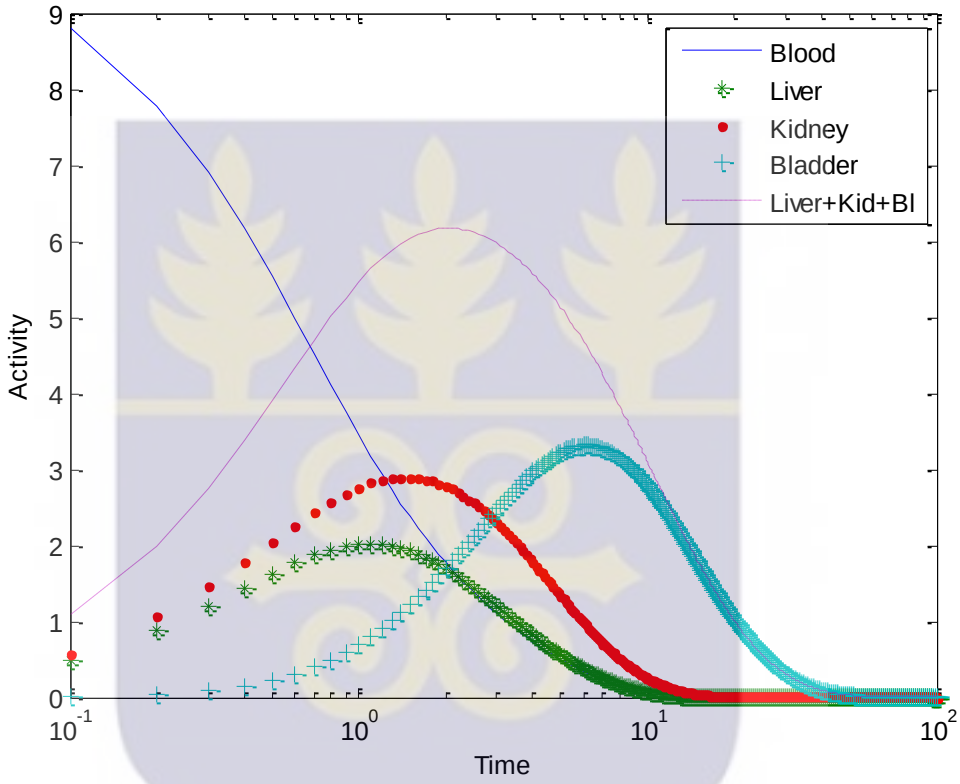

Figure 4.11: Time activity curve simulation for ^{99m}Tc-Sestamibi for blood, liver, kidney and bladder.

Figure 16 shows the simulated time-activity curve for blood, liver, kidney and the bladder. It was found that, the blood recorded a significant radionuclide activity of 10.00 mCi at the first minutes after injection of ^{99m}Tc-Sesamibi. This because^{99m}Tc-Sesamibi is injected directly into systemic circulation where the emission of gamma rays begins to occur before reaching the heart, kidney and the bladder. The bladder is a temporary urine reservoir, so the ^{99m}Tc-Sestamibi stays in the bladder for a relatively long period of time (about10 hours).The maximum uptake of the kidneys is

seen after 2 hours and the washout of liver is fast, and takes approximately one (1) hour.

4.2.6 Absorbed dose in different organs

The absorbed doses per unit of injected activity (mGy/MBq × 10^{-3}) were calculated with OLINDA methodfor source-organs (heart, urinary bladder, kidneys and liver) and target-organs (lung, spleen, testes and ovaries) .

Table 4.11: Comparison of Absorbed dose per administered activity with OLINDA and MIRDOSE 3

Target Organs	Absorbed Dose per Administered Activity (10^{-3}mGy/MBq)					
	Female			Male		
	MIRDOSE3	OLINDA	Difference %	MIRDOSE3	OLINDA	Difference %
Urinary Bladder	53.7	55.30	1.6	53.7	57.2	3.5
Kidneys	23.1	8.29	-14.8	23.1	7.25	-15.85
Liver	8.19	2.02	-6.17	8.19	3.63	-4.56
Heart	4.95	2.02	-2.93	4.95	1.93	-3.02
Thyroid	2.22	6.02	3.8	2.22	2.63	0.41
Spleen	8.62	4.90	-3.72	8.62	4.6	-4.02
Lung	2.75	2.48	-0.27	2.75	3.9	1.15
Testes	-	-	-	7.90	3.25	-4.65
Ovaries	62.4	54.6	-7.8	-	-	-

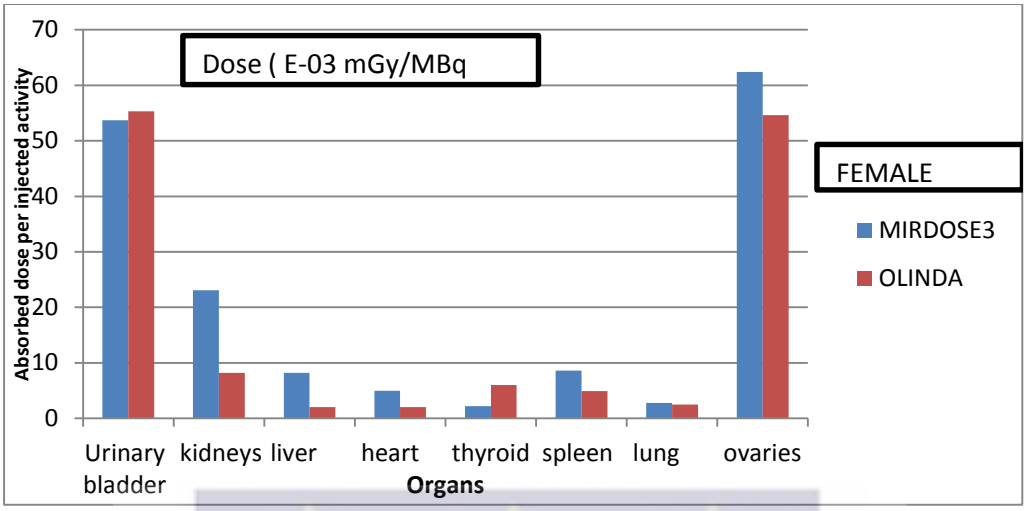

Figure 4.12:Absorbed dose per administered activity for female

Urinary bladder absorbed dose per administered activity for females' patient is relatively high and consequently the absorbed dose to the ovaries is also high.

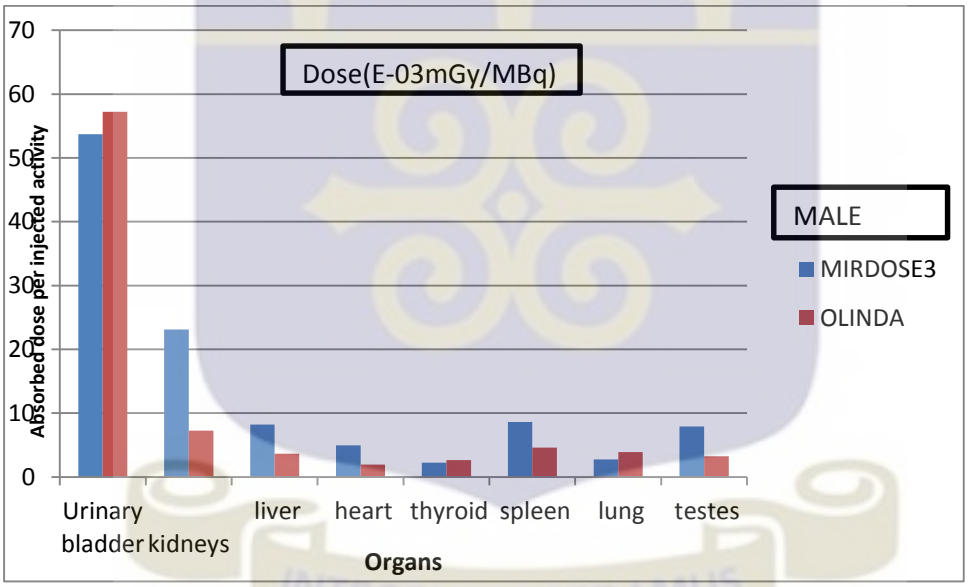

Figure 4.13: Absorbed dose per administered activity for male

Urinary bladder absorbed dose per administered activity for males' patient is relatively high but the absorbed dose to the testes is low.

This study focused on absorbed dose per unit of injected activity to organs of patients undergoing ^{99m}Tc-Sestamibi in the nuclear medicine department of Radioisotopes

institute in Niamey. The radionuclide activity in patient organs wasdetermined using the conjugate view method after scanning the patient. The absorbed doses per unit injected activity for patient target organs have been estimated. Internal radiation absorbed dose per administered activity for target organs of thirty patients was estimated by using OLINDA software and have been compared to the result of MIRDOSE 3 for ^{99m}Tc-Sestamibi. The Comparison of the data from the two methods shows that the difference is less than 10% except the kidneys which is about 15%.

The absorbed dose per unit administrated activity is relatively high for urinary bladder for both female and male patients and the dose to the ovaries is also high and low for the testes.

The absorbed dose per unit administered activity to patient organs found in this study was comparable to results from MIRDOSE 3 (Stabin, 1996).

4.2.7 Estimation of the uncertainties

Attenuation, Background and Scatter uncertainties

The linear attenuation coefficient of ^{99m}Tc in the water is 0.15/cm and the effective linear attenuation coefficient in tissue is 0.12/cm. The background uncertainty is calculated without subtracting the background and scatter uncertainty is found by removing 30% of the counts found in the organs because 20 – 40 % of the counts coming from the scatter. So the uncertainty was calculated by using the followed formula:

$$\frac{calculated\ value - theoritical\ value}{theoritical\ value} \text{x } 100 \quad (4.10)$$

Table 4.12 Estimation of uncertainties of the heart, liver, kidneys and bladder

Source-organs	Residence-time(τ)				Uncertainties
	With attenuation of 0.12/cm	With attenuation of 0.15/cm	Background	Scatter	
Heart	0.0807	0.1129			-28.52%
	0.0807		0.0356		126.68%
	0.0807			0.0935	-13.69%
Liver	0.2116	0.3018			-29.88%
	0.2116		0.0801		164.17%
	0.2116			0.2228	-5.02%
Kidneys	0.1017	0.1520			-33.09%
	0.1017		0.1289		-21.10%
	0.1017			0.1291	-21.22%
Urinary bladder	0.3367	0.4645			-27.53%
	0.3367		0.3410		-1.26%
	0.3367			0.0540	523.51%

Table 4.12 shows the estimated attenuation, background and scatter uncertainties in the heart, liver, kidneys and urinary bladder.

The negative values signified underestimated counts and overestimated for the positive values.

In this study, the three uncertainties were less than 40% except:

- Background uncertainty for heart and liver, with an overestimated of respectively 126.68% and 164.17%
- and scatter uncertainty for bladder with an overestimated of 523%.

The study shows that for heart and liver quantification, correction for background is very important and correction for scatter is no need for bladder quantification.According to Norrgren et al.2003, the effective attenuation coefficient correction influence the estimation of the activity by about ±10%, body thickness influence by about ±10%, device sensitivity by about ±5% and the background by about± 20%. So the uncertainty of attenuation correction can influence to about ±50%.

Delpon et al. 2003, found overestimated of up to 120% over the actual value of whole body activity in patient, using only attenuation correction. If scatter correction was performed in addition to attenuation correction, underestimates of 40±10% were observed.

CHAPTER FIVE: CONCLUSION AND RECOMMENDATION

5.1 Conclusion

Radionuclide activities in the heart, liver, kidney and bladder were estimated for ^{99m}Tc-Sestamibi imaging in SPECT myocardial perfusion imaging. The study was done at 10 minutes, 20 minutes, 2 hours and 4 hours after injection. Quantitative assessments of the uptakes in the organs of interest were performed from Scintigraphic scans from Mediso gamma camera. The InterViewXP® software was used for the drawing of ROIs and determining counts of activity. The ROIs were converted into activity using conjugate view method. The study involved thirty patients undergoing myocardial perfusion imaging in the Nuclear Medicine Department of AbdouMoumouni University (Niamey-NIGER). The cumulative radionuclide activities in the heart, liver, kidneys and urinary bladder were relatively low and represented about 1% of the injected activity.

The time-activity curve was simulated with MATLAB R2013a using biokinetic model publishedby Sydoff, 2013andRohe et al, 1995. These models were used to determine the theoretical activities in the blood, liver, and kidneys, four hours after injection, and two hours after injection in the bladder.

The residence times were estimatedfor the heart, liver, kidneys, and urinary bladder and were compared with the Mirdose 3 values published by Stabin, *1996*.

OLINDA was used to estimate radiation absorbed doses per administered activity and the results were comparable to the MIRDOSE3.

The radiation dose in organs of patients ‘undergoing myocardial perfusion was low. However, relatively high radiation absorbed dose was observed in the urinary bladder as a source-organ and in the ovaries as a target-organ.

5.2 Recommendations

Following the results obtained in this study, the following recommendations are made in cases of ^{99m}Tc-Sestamibi SPECT-MPI:

1- To patients;

Patients are encouraged to drink water and also to urinate frequently after injection of 99mTc-Sestamibi in order to reduce the activity level of the urine and the absorbed dose to the bladder.

2- To medical physicists

Medical physicists are encouraged to perform quantitative based researches in nuclear medicine dosimetry using protocols such as OLINDA, MIRDOSE to be able to accurately quantify dose to organs of patients undergoing scans.

REFERENCES

Agency, I. A. E.A (2011).Nuclear Medicine Physics.*Medical Physics*, *38*(8), 4904.

Ahasan, M.M. (2004). Assessment of radiation dose in Nuclear Medicine Hot Lab. *Iranian Journal of Radiation Research (Print)*, *2*(2), 75-78.

Alam et al, 2005. "Internal Dosimetry of Human Brain for ^{99m}-Tc and 131-I Using Nuclear Imaging in Bangladesh". Sri Lankan Journal of Physics.

Alam et al, 2011. "BIO-DISTRIBUTION AND DOSIMETRY OF A RENAL AGENT INNORMAL BANGLADESHI SUBJECTS" Bangladesh Journal of Medical Physics Vol. 4, No.1, 2011

Article, O. (2006). Myocardial uptake characteristics of three 99m Tc-labeled tracers for myocardial perfusion imaging one hour after rest injection, *20*(10), 663–670.

Bailey et al, 2013. An Evidence-Based Review of Quantitative SPECT Imaging and Potential Clinical Applications.*Journal of Nuclear Medicine*, *54*(1), 83–89.

Bambara et al,2015.ScienceDirect Estimation of kidney and bladder radionuclide activity for patients undergoing bone scan. *Journal of Radiation Research and Applied Sciences*, *8*(3), 317–322.

Bolch, W. E., Bouchet, L. G., Robertson, J. S., Wessels, B. W., Siegel, J. A., Howell, R. W., … Watson, E. E. (1998). MIRD Pamphlet No . 17 : The Dosimetry of Nonuniform Activity Distributionsâ€ " Radionuclide S Values at the Voxel Level.

Bolch, W. and Fahey, F.(2013). "The management of imaging procedure dose 2: Nuclear Medicine.Med. Phys. 40 (6), 486- 493 .

Buijs, W. C. A. M., Siegel, J. A., Boerman, O. C., &Corstens, F. H. (1998). Absolute organ activity estimated by five different methods of background correction. *Journal of Nuclear Medicine, 39,* 2167-2171.

Cardona, R. (2014) *Myocardial Perfusion SPECT*. Medscape [online]. [Accessed 21 October 2015]

Cristy M., Eckerman K.F., 1987. Specific Absorbed Fractions of Energy at Various Ages from Internal Photon Sources. Part I: Methods. ORNL Report TM-8381/V1. Oak Ridge National Laboratory, Oak Ridge, TN.

Darvish,(2013). Presentation and evaluation of gated-SPECT myocardial perfusion images Presentation and evaluation of gated-SPECT myocardial perfusion images.

David, A. W., Makler, P. T., Watson, E. E., Coffey, J. L., Thomas, S. R., and London, J. (1989). MIRD DOSE ESTIMATE REPORT NO 13 Radiation Absorbed Dose from Technetium-99m-Labeled Bone Imaging Agents. *Journal of Nuclear Medicine*, *30*(13), 1117–1123.

Dewaraja, Y. K., Wilderman, S. J., Ljungberg, M., Koral, K. F., Zasadny, K., and Kaminiski., M. S. (2005). Accurate Dosimetry in 131I Radionuclide Therapy Using Patient-Specific, 3-Dimensional Methods for SPECT Reconstruction and Absorbed Dose Calculation. *Journal of Nuclear Medicine*, *46*, 840–849.

Gahrouei, S. D., Cheki, M.,Moslehi, M. (2012). Estimation of organ absorbed doses in patients from 99mTc-diphosphonate using the data of MIRDose software. *Journal of Medical Signals and Sensors*, 2(4): 231-233.

Gurk, 2007. "Variation of image counts with patient anatomy and development of a Monte Carlo simulation system for whole-body bone scans."A thesis for Master of Science in Medical Physics, University of Canterbury.

Hatada et al, 2004. A New Myocardial Perfusion Imaging Agent with Rapid Liver Clearance: Comparison with 99mTc-Sestamibi and 99mTc-Tetrofosmin in Rats. *Journal of Nuclear Medicine*, *45*(12), 2095–2101.

Hays, M. T., Watson, E. E., Thomas, S. R., and Stabin, M. (2002). MIRD Dose Estimate Report No . 19 : Radiation Absorbed Dose Estimates from 18 F-FDG. *Journal of Nuclear Medicine*, *43*(19), 210–214.

Helal, N. (2012). Patient organs dose calculations in nuclear medicine. *International Journal of Research and Reviews in Applied Sciences*, *11*(April), 153–161.

Hendel, R. C., Berman, D. S., Di Carli, M. F., Heidenreich, P. A., Henkin, R. E., Pellikka, P. A., Williams, K. A. (2009). ACCF/ASNC/ACR/AHA/ASE/SCCT/SCMR/SNM 2009 appropriate use criteria for cardiac radionuclide imaging: a report of the American College of Cardiology Foundation Appropriate Use Criteria Task Force, the American Society of Nuclear Cardiology, the American Col. Circulation (Vol. 119). Retrieved from http://dx.doi.org/10.1016/j.jacc.2009.02.013

Hickson, J. K. (2011). Internal radionuclide dosimetry of model and patient based voxelised phantoms using the GATE toolkit. Royal Melbourne Institute of Technology.

Hou, X., Celler, A., Grimes, J., Bénard, F., and Ruth T., (2012).Theoretical dosimetry estimations for radioisotopes produced by proton-induced reactions on natural and enriched molybdenum targets, *Physics in medicine and biology 57 (6), 1499*.

Howard et al, 2011. "Comparison of I-131 Radioimmunotherapy Tumor Dosimetry: Unit Density Sphere Model Versus Patient-Specific Monte Carlo

Calculations". Cancer Biotherapy and Radiopharmaceuticals, Volume 26, Number 5, 2011, DOI: 10.1089/cbr.2011.0965.

International Atomic Energy Agency. (2014). Quantitative Nuclear Medicine Imaging: Concepts, Requirements and Methods. *IAEA HUMAN HEALTH REPORTS*, *9*, 59.

International Atomic Energy Agency, 2003."Standards and codes of practice in medical radiation dosimetry". Proceedings of an International Symposium Held in Vienna, Austria, 25–28 november 2002. Volume 2, International Atomic Energy Agency Vienna, 2003.

Inhibitor, G., Agrawal, M., Abraham, J., Balis, F. M., Edgerly, M., Stein, W. D., … Chen, C. C. (2003). Increased 99m Tc-Sestamibi Accumulation in Normal Liver and Drug-resistant Tumors after the Administration of the. *Clinical Cancer Research*, *9*, 650–656.

Jönsson, L. M. (2007). Internal Dosimetry Development and Evaluation of Methods and Models Medical Radiation Physics, Lund University.

Kári, B., Györke, T., Pártos, O., and Müller, I. (2004). *Handbook of InterViewXP Clinical guide of SPECT / Whole Body / Planar processing software package*. Budapest: MEDISO Medical Imaging Systems.

Konijnenberg, M. (2012). Physics and Radiation Exposure. In *99mTc-Sestamibi: Clinical Applications* (pp. 7–23). Berlin Heidelberg: Springer. doi:10.1007/978-3-642-04233-1

Li, W. B. andHoeschen, C.(2010).Uncertainty and sensitivity analysis of biokinetics models for radiopharmaceuticals used in Nuclear Medicine.Radiation Protection Dosimetry, 139 (1-3), 228-23.1.

Liu, S, He Z., Hsieh, W. Y., Kim Y. S. (2006) Evaluation of novel cationic (99m) Tc-nitrido complexes as radiopharmaceuticals for heart imaging: improving liver clearance with crown ether groups. Nucl Med Biol, 33:419–432.

MallinckrodtPharmaceuticals (2015). *Tc 99m Sestamibi Injection Full Prescribing Information : Contents * 1 Indications and usage 7 Drug Interactions Note : References How Supplied / Storage And Handling* (Vol. 10), 4-5, Maryland.

Melendez, L. A., Rodriguez, J. C., Ferro F. G., Consuelo, M. A., Herrera, R., Rodriguez, E., Mitsoura, C., Martinez, D. (2004). Biokinetics of 99m Tc-UBI 29-41 in humans. Nucl Med Biol, 31,373-379.

Monsieurs, M. (2010). Patient dosimetry and radiation protection issues for radionuclide therapy using 131 I. Thesis submitted to the department of Anatomy, Embryology, Histology and Medical to obtain the degree of Doctor in Medical Sciences, Ghent University.

Pereira, J. M.,Stabin,M. G., Lima, F. R. A., Guimarães, M. I. C. C., Forrester, J. W. (2010).Image Quantification for Radiation Dose Calculations - Limitations andUncertainties. Health Physics 99:5, 688-701

Robinson, M. S., Colas-linhart, N. C., Guiraud-vitaux, F., Petiet, A. M., and Bok, B. D. (1997). Heterogeneous Distribution of Technetium-99m-Labeled Microspheres in Rat Lungs : Microautoradiographic Evidence and Dosimetrie Consequences nnI. *The Journal of Nuclear Medicine, 38*(4), 650– 654.

Rohe R. C, Thomas S. R., Stabin M. G.,Deutsch, E. A., Gerson, M. C., Cummings, D. D., and Maxon H. R.(1995). Biokinetics and dosimetry analysis inhealthy volunteers for a two-injection (rest-stress) protocol of the myocardial perfusion imaging agent technetium 99m-labeled Q3. J NuclCardiol, 2, 395–404.

Sadik, M. (2009). Computer-Assisted Diagnosis for the Interpretation of Bone Scintigraphy: A new approach to improve diagnostic accuracy. Gothenburg: GesonHylteTryck.

Sahebnasagh, A., Adinehvand, K., and Azadbakht, B. (2012). Determination and Comparison of Absorbed dose of Ovaries and Uterus in Heart Scan from TC-99m, by Three Methods : TLD Measurement , MCNP Simulation and MIRD Calculation and Estimation of its Risks. *Research Journal of Applied Sciences, Engineering and Technology, 4(22), 4572–4575.*

Savi, A, Gerundino, P, Zoli, P.,Maffioli, L., Compierchio, A., Colombo, F., Matarrese, M.and Deutsch, E. (1989).Biodistribution of Tc-99m methoxy-isobutyl-isonitrile (MIBI) in humans. Eur J Nucl Med.15:597–600.

Sgouros, G., Squeri, S., Ballangrud, Å. M., Kolbert, K. S., Teitcher, J. B., Panageas, K. S., … Zelenetz, A. D. (2003). Non-Hodgkin ' s Lymphoma Patients Treated with 131 I-anti-B1 Antibody : Assessment of Tumor Dose – Response. *The Journal of Nuclear Medicine, 44*(2), 260–268.

Siegel, J. A., Thomas, S. R., Stubbs, J. B., Stabin, M. G., Hays, M. T., Koral, K. F., Brill, A. B. (1999). MIRD Pamphlet No . 16 : Techniques for Quantitative Radiopharmaceutical Biodistribution Data Acquisition and Analysis for Use in Human Radiation Dose Estimates. *Journal of Clinical Imaging, 40*(16), 37–61.

Smith, E. M., Anger, E. M., Harris, E. M. and Mitchel, E. M.(1967). Internal radiation dosimetry.*Environmental Health Series. [RH] Radiological Health, 3001*, 45–53.

Stabin, M. G. (2009). *Internal Dose Assessment in Nuclear Medicine* (Vol. 14). Albuquerque: University of New Mexico Health Sciences Center.

Stabin, M. G., and Flux, G. D. (2007). Internal dosimetry as a tool for radiation protection of the patient in nuclear medicine. *Biomedical Imaging and Interventional Journal*, *3*(2), 1–11. http://doi.org/10.2349/biij.3.2.e28

Stabin, M. G., Sparks, R. B. and Crowe, E (1996). MIRDOSE: Personal computer software for internal dose assessment innuclear medicine, J. Nucl. Med. 37(3), 538–546

Stabin, M. G. (2008). The Importance of Patient-Specific Dose Calculations in Nuclear Medicine. *Nuclear Engineering and Technology*, *40*(7), 527–532.

Stabin, M. G. (2008) Fundamentals of Nuclear Medicine Dosimetry. Springer, New York, NY.

Stabin, M. G.(2006).Nuclear medicine dosimetry.*Physics in Medicine and Biology*.

Stabin, M. G.(2005).OLINDA/EXM: The Second-Generation Personal Computer Software for Internal Dose Assessment in Nuclear Medicine". J Nucl Med 2005; 46:1023–1027.

Stabin, M. G. (2008). Uncertainties in internal dose calculations for radiopharmaceuticals. J Nucl Med; 49 (5),1–60.

Sydoff, M. (2013). Quantification Methods for Clinical Studies in Nuclear Medicine - Applications in AMS, PET/CT and SPECT/CT Lund University, dept. of Medical Radiation Physics

Snyder, W. S., Ford, M. R., Warner, G. G., and Watson, S. B. (1975). MIRD Pamphlet 11: "S," Absorbed dose per unit cumulated activity for selected radionuclides and organs 1-69.pdf. New York: Society of Nuclear Medicine.

Snyder, W. S., Ford, M. R., and Warner, G. G. (1978). *nm/MIRD Pamphlet 5: Estimates of Specific Absorbed fractions for Phototn sources uniformly distrinuted in various Organs of a Heterogeneous Phantom*. New York: Society of Nuclear Medicine.

Wackers, F. J. T., Berman, D. S., Watson, D. D., Beller, G. A., Strauss, H. W., Boucher, C. A., … Mckusick, K. (2016). Technetium-9 9m Hexakis 2-Methoxyisobutyl Isonitrile : Human Biodistribution , Dosimetry , Safety , and Preliminary Comparison to Thaffium-201 for Myocardial Perfusion Imaging. *Journal of Nuclear Medicine*, *30*(3), 301–312.

Zanzonico, P. B. (2000). Internal Radionuclide Radiation Dosimetry : A Review of Basic Concepts and Recent Developments *. *Journal of Nuclear Medicine*, *41*, 297–308.

APPENDIX

Appendix 1: Body and organs Thickness (cm)

		Thoraco-abdominal		Abdomino-pelvic	
Patient #	**Thickness**	**Heart**	**Liver**	**Kidneys**	**Bladder**
	A/P Body section	22.0	23.0	21.5	25.1
1	A/P Organ	9.00	16.20	4.6	7.70
	A/P Body section	23.1	24.1	20.7	24.2
2	A/P Organ	10.2	14.70	5.2	8.50
	A/P Body section	21.6	23.6	19.5	22.6
3	A/P Organ	11.8	15.90	5.8	9.40
	A/P Body section	22.8	20.1	23.0	21.8
4	A/P Organ	8.6	17.60	5.4	10.0
	A/P Body section	22.6	19.8	22.4	20.6
5	A/P Organ	9.90	13.80	5.8	8.20
	A/P Body section	19.0	21.0	21.0	25.8
6	A/P Organ	8.90	14.00	5.2	7.80
	A/P Body section	20.6	20.8	19.4	21.4
7	A/P Organ	8.80	16.80	6.0	7.50
	A/P Body section	21.6	22.0	18.9	20.9
8	A/P Organ	9.70	17.20	4.7	8.00
9	A/P Body section	22.9	21.3	21.2	24.6
	A/P Organ	9.30	16.60	6.2	8.60
	A/P Body section	22.8	23.3	22.4	23.0
10	A/P Organ	10.8	14.20	6.1	9.3

Appendix2: Activity of the heart and liver 10 minutes after injection of 99mTc-Sestamibi

Nº	Heart Ant	Ant Backg	Heart post	Post Backg	Liver Ant	Ant Backg	Liver post	Post Backg	Heart GMC	Liver GMC	Heart Activity(µCi)	Liver Activity(µCi)
1	31091	5000	21051	4000	183288	10000	144281	8000	21092.12	485961.53	208.57	1328.04
2	34003	5000	26076	4000	136405	10000	91070	8000	80014.18	102471.76	250.21	885.55
3	23710	5000	20691	4000	123095	10000	99454	8000	17671.68	101700.49	174.75	878.89
4	24835	5000	18302	4000	164373	10000	146036	8000	9147.68	145976.13	166.55	1261.51
5	27888	5000	26552	4000	188585	10000	144104	8000	22719.37	155904.24	224.66	1347.31
6	28406	5000	22377	4000	181301	10000	165600	8000	20739.62	164307.75	205.08	1419.93
7	24263	5000	18060	4000	83593	10000	73215	8000	16457.14	69277.46	162.74	598.69
8	29619	5000	28174	4000	72416	10000	60127	8000	24395.48	57039.97	241.23	492.93
9	30649	5000	27702	4000	106867	10000	93402	8000	24656.28	90954.02	243.81	786.02
10	19253	5000	17504	4000	81407	10000	69015	8000	13873.44	66006.80	137.19	570.42
11	30965	5000	27071	4000	124171	10000	109291	8000	24475.26	107538.34	242.02	929.34
12	29492	5000	28172	4000	191202	10000	157654	8000	24331.47	164674.23	240.60	1423.10
13	33805	5000	30562	4000	189801	10000	167071	8000	27660.77	169118.67	273.52	1461.51
14	24640	5000	21620	4000	131380	10000	117130	8000	18602.60	115092.13	183.95	994.61
15	35919	5000	27439	4000	193253	10000	165970	8000	26920.44	170142.51	266.20	1470.36
16	31404	5000	28025	4000	132605	10000	124297	8000	25186.42	119409.35	249.06	1031.92
17	21912	5000	19794	4000	113027	10000	100316	8000	16343.44	97524.56	161.61	842.80

18	12836	5000	11808	4000	69123	10000	59353	8000	7821.98	55101.21	77.35	476.18
19	20854	5000	20186	4000	94338	10000	84323	8000	16019.13	80230.47	158.40	693.34
20	36245	5000	34318	4000	140282	10000	130282	8000	30778.01	131278.19	304.35	1134.49
21	24107	5000	23351	4000	144773	10000	131205	8000	19228.61	128859.25	190.14	1113.59
22	31212	5000	27146	4000	212026	10000	203576	8000	24631.34	198774.83	243.57	1717.79
23	47196	5000	42507	4000	126310	10000	116042	8000	40309.32	112099.79	398.60	968.76

Effective linear attenuation: 0.12/cm Liver F: 0.4007 Heart F: 0.4585

Calibration factor: 172.8 CPM/μCi

Expμe:0.072 for heart and liver

Appendix3: Activity of the bladder 10 minutes after injection of 10 mCi of 99mTc-Sestamibi

Nº	Anterior	Background	Posterior	Background	GMC	Activity
1	89815	5000	87327	5000	83561.74	899.46
2	96504	5000	95834	5000	91168	981.33
3	71302	5000	61126	5000	61002.18	656.63
4	86489	5000	75139	5000	75601.30	813.77
5	31199	5000	30725	5000	25960.91	279.44
6	18178	5000	17032	5000	12591.96	135.54
7	49217	5000	33649	5000	35591.75	383.11

Effective linear attenuation: 0.12/cm Bladder F: 0.4676

Calibration factor: 172.8 CPM/µCi

Expµe:0.0632 for Bladder

Appendix 4: Matlab code

```
A=[-1.295 0.76 0.02 0; 0.55 -2.675 0 0; 0.63 0 -0.535 0; 0 0 0.40 -0.115];
x0 = [10 0 0 0]';
B = [0 0 0 0]';
C = [1 0 0 0];
D = 0;
fori = 1:1001,
u(i) = 0;
t(i) = (i-1)*0.1;
end;
sys=ss(A,B,C,D);
[y,t,x] = lsim(sys,u,t,x0);
plot(t,x(:,1),'-',t,x(:,2),'*',t,x(:,3),'.',t,x(:,4),'+',t,x(:,2)+x(:,3)+x(:,4),':')
semilogx(t,x(:,1),'-',t,x(:,2),'*',t,x(:,3),'.',t,x(:,4),'+',t,x(:,2)+x(:,3)+x(:,4),':')
legend('Blood','Liver','Kidney','Bladder','Liver+Kid+Bl')
% save data
n = length(t);
fid = fopen('gi44chaineq.txt','w'); % Open a file to be written
fori = 1:n,
fprintf(fid,'%10.8f %20.16f %20.16f %20.16f %20.16f %20.16f\n',t(i),x(i,1),x(i,2),x(i,3),x(i,4),x(i,2)+x(i,3)+x(i,4)); % Saving data
end
% d1 activity in blood after 4h
% d2 activity in liver after 4h
% d3 activity in kidney after 4h
% d4 activity in Urinary Bladder after 2h
d1=x(31,1)
d2=x(31,2)
d3=x(31,3)
d4=x(31,4)
fclose(fid);
savegi44chaineq.dat-asciit,x
```